HAL
open science

Phase transition in time-reversible Navier-Stokes equations

Vishwanath Shukla, Bérengère Dubrulle, Sergey Nazarenko, Giorgio Krstulovic, Simon Thalabard

To cite this version:

Vishwanath Shukla, Bérengère Dubrulle, Sergey Nazarenko, Giorgio Krstulovic, Simon Thalabard. Phase transition in time-reversible Navier-Stokes equations. Physical Review E , 2019, 100 (4), 10.1103/PhysRevE.100.043104 . hal-02346672

HAL Id: hal-02346672

https://hal.science/hal-02346672v1

Submitted on 5 Nov 2019

HAL is a multi-disciplinary open access archive for the deposit and dissemination of scientific research documents, whether they are published or not. The documents may come from teaching and research institutions in France or abroad, or from public or private research centers.

L'archive ouverte pluridisciplinaire **HAL**, est destinée au dépôt et à la diffusion de documents scientifiques de niveau recherche, publiés ou non, émanant des établissements d'enseignement et de recherche français ou étrangers, des laboratoires publics ou privés.

Phase transition in time-reversible Navier-Stokes equations

Vishwanath Shukla,[1,2,*] Bérengère Dubrulle,[3] Sergey Nazarenko,[2] Giorgio Krstulovic,[4] and Simon Thalabard[5,†]

[1] *Department of Physics, Indian Institute of Technology Kharagpur, Kharagpur 721302, India.*
[2] *Université Côte d'Azur, Institut de Physique de Nice (INPHYNI), CNRS UMR 7010, Parc Valrose, 06108 Nice Cedex 2, France*
[3] *DSM/IRAMIS/SPEC, CNRS UMR 3680, CEA, Université Paris-Saclay, 91190 Gif sur Yvette, France*
[4] *Université Côte d'Azur, CNRS, OCA, Laboratoire Lagrange, Bd. de l'Observatoire, Nice, France*
[5] *Instituto Nacional de Matemática Pura e Aplicada, IMPA, 22460-320 Rio de Janeiro, Brazil*

(Dated: July 23, 2019)

We present a comprehensive study of the statistical features of a three-dimensional time-reversible Navier-Stokes (RNS) system, wherein the standard viscosity ν is replaced by a fluctuating thermostat that dynamically compensates for fluctuations in the total energy. We analyze the statistical features of the RNS steady states in terms of a non-negative dimensionless control parameter $\mathcal{R}_{\rm r}$, which quantifies the balance between the fluctuations of kinetic energy at the forcing length scale $\ell_{\rm f}$ and the total energy E_0. For small $\mathcal{R}_{\rm r}$, the RNS equations are found to produce "warm" stationary statistics, *e.g.* characterized by the partial thermalization of the small length-scales. For large $\mathcal{R}_{\rm r}$, the stationary solutions have features akin to standard hydrodynamic ones: They have compact energy support in k-space and are essentially insensitive to the truncation scale $k_{\rm max}$. The transition between the two statistical regimes is observed to be smooth but rather sharp. Using insights from a diffusion model of turbulence (Leith model), we argue that the transition is in fact akin to a *continuous phase transition*, where $\mathcal{R}_{\rm r}$ indeed behaves as a thermodynamic control parameter, *e.g.* a temperature. A relevant order-parameter can be suitably defined in terms of a (normalized) enstrophy, while the symmetry breaking parameter h is identified as (one over) the truncation scale $k_{\rm max}$. We find that the signatures of the phase transition close to the critical point $\mathcal{R}_{\rm r}^\star$ can essentially be deduced from a heuristic mean-field Landau free energy. This point of view allows us to reinterpret the relevant asymptotics in which the *dynamical ensemble equivalence* conjectured by Gallavotti, *Phys.Lett.A, 223, 1996* could hold true. We argue that Gallavotti's limit is precisely the joint limit $\mathcal{R}_{\rm r} \overset{>}{\to} \mathcal{R}_{\rm r}^\star$ and $h \overset{>}{\to} 0$, with the overset symbol "$>$" indicating that these limits are approached from above. The limit therefore relates to the statistical features at the critical point. In this regime, our numerics indicate that the low-order statistics of the 3D RNS are indeed qualitatively similar to those observed in direct numerical simulations of the standard Navier-Stokes (NS) equations with viscosity chosen so as to match the average value of the reversible viscosity. This result suggests that Gallavotti's *equivalence conjecture* could indeed be of relevance to model 3D turbulent statistics, and provides a clear guideline for further numerical investigations at higher resolutions.

Keywords: turbulence; irreversibility; direct numerical simulations; dynamical ensembles equivalence

arXiv:1811.11503v2 [physics.flu-dyn] 20 Jul 2019

I. INTRODUCTION

Describing the irreversible behaviors of macroscopic observables arising from time-reversible microscopic dynamics is the central long-standing theme of non-equilibrium statistical mechanics [1–3]. When there exists a wide scale separation between the microscopic and the macroscopic scales, the emergence of irreversibility can in general be formalized using a variety of reduction techniques including but not limited to stochastic equations, diffusion or projection operator formalisms that model the collective evolution of the fast variables [4–7]. The scope of many other promising strategies is still an active area of research [8–12]; therefore, a systematic framework is lacking that allows to derive, from first principles, a non-equilibrium thermodynamic formalism to account for the macroscopic irreversibility.

In the context of three-dimensional (3D) stationary homogeneous isotropic turbulence, a hallmark of irreversibility is the phenomenon of anomalous dissipation, namely the fact that the rate of energy dissipation ϵ becomes finite as the separation between the injection and the dissipative viscous scales become infinite. The breaking of detailed balance is then made apparent through the celebrated four-fifth law (see, e.g. Ref. [13]), which ties ϵ to the average of the cube of the longitudinal velocity increments. This is an anomalous feature, as in the limit of vanishing viscosity (infinite Reynolds number) the flow could in principle formally be described by the time-symmetric Euler equations.

A thorough description of irreversibility in turbulence requires to underpin its precise features and in recent years this problem has witnessed a renewed interest. In particular, non-trivial signatures of irreversibility have been identified on the Lagrangian statistics: Both experiments and large numerical simulations have demonstrated that these depend on the forward-in-time or backward-in-time conditioning [14–17]. For instance,

* research.vishwanath@gmail.com
† simon.thalabard@impa.br

both fluid and heavy particles tend to gain kinetic energy slowly but loose it rapidly along their Lagrangian trajectories [18–20]: This is a clear example of an irreversible behavior, whose origin is related to the vortex stretching and generation of small length scales [21]; this persists even in the limit of vanishing viscosity.

One important difficulty in studying turbulent irreversibility comes from its asymptotic nature. Even massive computational effort in numerically integrating the NS equations may fail in clearly disentangling the finite-Reynolds-number effects from its truly asymptotic features [22, 23]. An alternative approach is to modify the governing equations to make them time-reversible, and then study whether the irreversible signatures of turbulence are still present under suitably defined limits. An early example of such an approach is that of the "constrained Euler system" considered in Ref. [24], wherein the energies contained within narrow wave number shells are held constant in time. The resulting system was shown to reproduce many of the standard statistical features of isotropic Navier-Stokes (NS) turbulence, including intermittency.

In Ref. [25], another time-reversible governing equation was proposed, based on the assumption that the fluid is not subjected to the usual viscous dissipation, but rather to a modified dissipation mechanism, obtained by imposing a global constraint on the system. This results in a time-reversal invariant dissipative term characterized by the appearance of a "reversible viscosity" that balances the energy injection by behaving like a "thermostatting term", while a prescribed macroscopic observable such as the total energy or the total enstrophy remains constant in time. An equivalence between these time-reversible formulations and the standard NS dynamics was postulated to hold true in the limit of high Reynolds number [25], as a consequence of a more general *equivalence of dynamical ensembles* for non-equilibrium systems [26]. If this "equivalence conjecture" is true, at least for suitable choices of thermostat, then the statistical features of turbulent flows in the inertial range can be obtained by adopting two distinct approaches, which model microscopic dissipation differently, but yield an equivalent macroscopic behavior.

The use of the reversible formulation opens up the possibility to explore the implications of the chaotic hypothesis [27] for the fluctuations of the local observables and the Lyapunov spectrum. This perspective has motivated many investigations, including numerical [28–31] and experimental ones [32].

Numerical tests probing the equivalence of dynamical ensembles have been performed in various settings, but so far only for simple models rather than the full 3D NS equations. For instance, the time-reversible version of the shell model of turbulence obtained by imposing a global constraint of energy conservation was investigated in [28]. It was found that as the amplitude of the external force is varied, from zero to high values, the system exhibits a smooth transition from an equilibrium state to a non-equilibrium stationary state with an energy cascade from large to small scales.

Such models have also been studied in combination with various kinds of thermostats. Recent results suggest that the relevance of the equivalence conjecture might crucially depend on which macroscopic observable is chosen to be held constant [33, 34]. Insights on how macroscopic irreversibility is linked to the non-equilibrium energy cascade process rather than to the explicit breaking of the time-reversal invariance due to viscous dissipation were also reported in Ref. [35].

The validity of the equivalence conjecture along with various consequences of the chaotic hypothesis were tested for incompressible two-dimensional (2D) flows [29, 31]. Direct numerical simulations (DNS) of the incompressible 2D NS equations were compared to their reversible counterpart, in order to examine the fluctuations of global quadratic quantities in statistically stationary states. A comparative study of the Lyapunov spectra showed that they overlap [31]. These studies naturally went beyond the reduced models of turbulence and dealt with the full governing equations, though with small number of Fourier modes, and provided an additional support in favor of the conjecture.

The above discussion suggests that the (time) Reversible Navier-Stokes (RNS) systems, as prescribed by the equivalence conjecture, can perhaps provide a generalized framework which is capable of producing genuine turbulent statistics arsing from a time-reversible dynamics. This is especially useful for understanding the anomalous turbulent signatures. Therefore, the recent works based on the shell models of turbulence [33, 35] are a step forward in understanding the Gallavotti's conjecture.

To the best our knowledge, no systematic attempt has been made so far in order to clearly achieve the limit in which the equivalence conjecture could supposedly hold true, *e.g.* the limit $\nu \to 0$ for the *full* 3D NS equations. The obvious reason for this, is the fact that this question is both subtle and *a priori* difficult to tackle from a numerical perspective. Any numerical scheme involves a cutoff scale $k_{\max}$, and the desired asymptotics is then necessarily a joint limit $k_{\max} \to \infty$, $\nu \to 0$. In principle, these two limits do not commute. In the context of Gallavotti's original equivalence conjecture, one should clearly let $k_{\max} \to \infty$ before letting $\nu \to 0$, and in our view even a phenomenological hint as to whether the equivalence conjecture should reasonably hold in this limit is perhaps currently lacking. To gain such an intuition, one should probably first understand the nature of statistical regimes that the RNS dynamics is likely to generate. Yet, systematic overviews, to this day, at best are either essentially qualitative or simply absent, especially for the case of 3D RNS. The present paper intends to fill this gap.

Our work offers a comprehensive study of the statisti-

cal features of a 3D time-reversible NS system, in which the standard viscosity is replaced by a fluctuating thermostat that dynamically compensates for fluctuations in the total energy. To identify different statistical regimes of this system, we introduce a non-negative dimensionless control parameter $\mathcal{R}_{\rm r} = f_0\ell_{\rm f}/E_0$, which quantifies the balance between the injection of kinetic energy at the forcing length-scale $\ell_{\rm f}$ and the total energy E_0. We find that the system exhibits a smooth transition from a high-enstrophy, truncation effects dominated phase at small $\mathcal{R}_{\rm r}$ to low-enstrophy, hydrodynamical states at large $\mathcal{R}_{\rm r}$. This transition has features akin to a continuous phase transition, with average enstrophy as an order parameter.

For small values of $\mathcal{R}_{\rm r}$, the RNS equations produce steady states that exhibit close-to-equilibrium Gibbs-type statistics at small length-scales. Following Ref. [36], we refer to such states as *warm* states (solutions). The terminology is simply meant to convey the idea that the spectra being partially thermalized at the ultra-violet end, should behave akin to a heat-bath, a feature previously observed in truncated fluid models [37–39]. For large $\mathcal{R}_{\rm r}$, the stationary solutions have compact energy support in k-space and are found to be essentially insensitive to the cutoff scale $k_{\rm max}$ (later precisely defined) and we refer to these kind of states as being of *hydrodynamic* type. Furthermore, using insights from a reversible non-linear diffusion model of turbulence (Leith model), we argue that the transition is in fact akin to a *continuous phase transition*, and that $\mathcal{R}_{\rm r}$ indeed behaves as a thermodynamic control parameter, *e.g.* a temperature. Also, as mentioned above, a relevant order-parameter can be suitably defined in terms of a (normalized) enstrophy, while the symmetry breaking parameter h is identified as (one over) the truncation scale $k_{\rm max}$. We find that the signatures of the phase transition close to the critical point $\mathcal{R}_{\rm r}^\star$ can essentially be deduced from a heuristic mean-field Landau free energy. This point of view allows us to reinterpret the relevant asymptotics in which Gallavotti's conjecture could hold true. Gallavotti's limit precisely corresponds to the joint limit $\mathcal{R}_{\rm r} \overset{>}{\to} \mathcal{R}_{\rm r}^\star$ and $h \overset{>}{\to} 0$, with overset "$>$" meaning that the critical point is approached from above. It therefore relates to the statistics in the neighborhood of the critical point. In this regime, our numerics indicate that the 3D RNS steady statistics mimic their standard NS counterpart, with viscosity matching the average value of the reversible viscosity. This result hints towards the validity of the equivalence conjecture.

The remainder of this paper is organized as follows. § II introduces the RNS equations and the control parameter $\mathcal{R}_{\rm r}$. We schematically discuss the expected statistical features of the RNS states in the two opposite asymptotic limits: $\mathcal{R}_{\rm r} \to 0$ and $\mathcal{R}_{\rm r} \to \infty$. § III describes the outcomes of our RNS numerics, and presents a detailed overview of the different statistical regimes which we observe. We identify a small crossover range of $\mathcal{R}_{\rm r}$, wherein the RNS states continuously transits from being "warm" to "hydrodynamic". § IV discusses insights obtained from the analysis of a suitably defined "reversible Leith model", the statistical regimes of which are interpreted within the framework of a mean-field second-order Landau theory. § V extends the discussion to the RNS system, and reformulates the equivalence in a thermodynamic framework. We compare low-order RNS and NS statistics at values of $\mathcal{R}_{\rm r}$ that are slightly above the critical point, and argue that this is indeed the relevant regime to consider. § VI summarizes our findings and presents some perspectives.

II. THE (TIME) REVERSIBLE NAVIER-STOKES EQUATIONS

A. Formal definitions

The spatio-temporal evolution of the velocity field $\mathbf{u}(\mathbf{x},t)$ describing an incompressible fluid flow within a spatial domain $\mathcal{D}$ is governed by the Navier-Stokes (NS) equations

$$\frac{\partial \mathbf{u}}{\partial t} + (\mathbf{u}\cdot\nabla)\,\mathbf{u} = -\nabla p + \nu\nabla^2\mathbf{u} + \mathbf{f}, \tag{1}$$

where ν is the kinematic viscosity, p is the pressure field and $\mathbf{f}$ is the forcing term, acting at large length-scales, to sustain a statistically steady state. The incompressibility is ensured by requiring $\nabla\cdot\mathbf{u} = 0$ and the fluid density is set to 1.

In presence of the viscous dissipation term $\nu\nabla^2\mathbf{u}$, the resulting macroscopic dynamics is clearly irreversible, as the NS equations (1) are not invariant under the transformation

$$\mathcal{T}:\, t \to -t;\, \mathbf{u} \to -\mathbf{u}. \tag{2}$$

We now follow Ref. [25], and alter the dissipation operator term to make it invariant under the transformation $\mathcal{T}$. The modification consists in transforming the dissipation operator into a thermostat, so that a certain macroscopic quantity, such as the total energy or the total enstrophy, becomes a conserved quantity. While Ref. [40] discusses several implementations of this idea, we here choose to follow Ref. [28, 29], and impose a constraint on the total kinetic energy. An elementary calculation shows that in order for the energy to be held constant, the viscosity must fluctuate as

$$\nu_{\rm r}[\mathbf{u}] = \frac{\int_{\mathcal{D}} \mathbf{f}\cdot\mathbf{u}\,d\mathbf{x}}{\int_{\mathcal{D}} (\nabla\times\mathbf{u})^2\,d\mathbf{x}}. \tag{3}$$

The "reversible viscosity" is a functional of $\mathbf{u}$ and depends on the state of the system. We refer to the equations obtained by replacing the constant in time viscosity ν in the NS equations (1) with the state dependent $\nu_{\rm r}$ as the "Reversible Navier-Stokes" (RNS) equations:

$$\frac{\partial \mathbf{u}}{\partial t} + (\mathbf{u}\cdot\nabla)\,\mathbf{u} = -\nabla p + \nu_{\rm r}\nabla^2\mathbf{u} + \mathbf{f}, \tag{4}$$

where we still enforce incompressibility as $\nabla \cdot \mathbf{u} = 0$.

B. Control parameter $\mathcal{R}_\mathrm{r}$

To characterize the statistical steady states of the RNS system, we use the dimensionless control parameter

$$\mathcal{R}_\mathrm{r} = \frac{f_0 \ell_\mathrm{f}}{E_0}, \tag{5}$$

where E_0 is the total (conserved) energy fixed by the initial state, f_0 is the forcing amplitude and ℓ_f is the energy injection length scale.

Despite its suggestive name, the control parameter $\mathcal{R}_\mathrm{r}$ should not be interpreted as either a "Reversible Reynolds number" or an inverse thereof : None of the two asymptotic regimes $\mathcal{R}_\mathrm{r} \to 0$ and $\mathcal{R}_\mathrm{r} \to \infty$ describe a fully-developed turbulent state. This is perhaps slightly counter-intuitive as when $\mathcal{R}_\mathrm{r} \to 0$ the RNS dynamics formally reduces to the freely evolving Euler equations. There is yet no reason to expect this limit to produce a "fully developed turbulent" steady state, as it corresponds to a very specific *joint limit*, where both the viscous and the forcing term simultaneously vanish. Fully developed turbulence is in principle generated from the NS equations in a different manner, that is by letting the standard viscosity $\nu \to 0$ at fixed value of the forcing f_0 [13]. There is therefore no reason that both limits coincide.

The present work relies on numerical integration of the RNS equations. The fact that the limit $\mathcal{R}_\mathrm{r} \to 0$ is not linked with the fully-developed turbulence becomes clear from the following arguments. Indeed, any numerical calculation involves a finite resolution, or equivalently a finite number of degrees of freedom. At fixed resolution, the limit $\mathcal{R}_\mathrm{r} \to 0$ does not yield the Euler equations but rather their *truncated* counterpart. Hence, the numerical integration of the truncated RNS equations, in the limit $\mathcal{R}_\mathrm{r} \to 0$, will converge towards an *absolute equilibrium equipartition state* that corresponds to the equipartition of energy among the modes; this state has Gaussian statistics quite unlike a fully developed turbulent state. We refer the reader to Appendix A for further details on absolute equilibria and truncated Euler flows.

The limit $\mathcal{R}_\mathrm{r} \to \infty$, on the contrary, resembles an over-damped dynamics: In this limit, the forcing is infinitely large compared to the energy retained in the system. Therefore, any energy injected at length-scale ℓ_f should in principle be immediately removed by the reversible viscosity, thereby suppressing the nonlinear transfer of energy. This asymptotic steady state is mostly insensitive to the number of modes used in the numerical simulations.

The two asymptotic phases should obviously cross over at intermediate values of $\mathcal{R}_\mathrm{r}$, and this is very schematically summarized by the diagram sketched in Fig. 1. Our numerical simulations intend to substantiate this crude phenomenological overview, and in particular provide a detailed characterization of the RNS statistical regimes when $\mathcal{R}_\mathrm{r}$ takes a finite value.

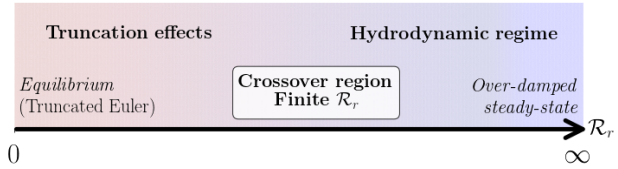

FIG. 1. A schematic illustration of the phase diagram of the (truncated) RNS system. The small $\mathcal{R}_\mathrm{r}$ truncation dominated regime and the large $\mathcal{R}_\mathrm{r}$ hydrodynamic regimes are separated by a crossover region, in accordance with the heuristic description of § II B based on the two asymptotic limits $\mathcal{R}_\mathrm{r} \to 0$ and $\mathcal{R}_\mathrm{r} \to \infty$.

III. NUMERICAL EXPERIMENTS

We begin this section with a brief overview of our numerical methods that we use to study the RNS system, followed by a comprehensive description of the results obtained from the numerical simulations. We show that the phase diagram depicted in Fig. 1 is correct. The RNS system indeed has two distinct statistical regimes separated by a crossover region; the transition between these two regimes has the character of a continuous-phase transition.

A. Details of the simulations

1. *Numerical schemes*

We perform numerical simulations of the 3D NS Eqs. (1) and the 3D RNS Eqs. (4) by using the Fourier pseudo-spectral method, implemented in an efficient, parallel numerical code VIKSHOBHA [41].

The velocity field $\mathbf{u}$ is solved inside a cubic domain $\mathcal{D}$ of side 2π, and is prescribed to be triply-periodic. Therefore, it can be represented by the Fourier series

$$\mathbf{u}(\mathbf{x}, t) = \sum_{\mathbf{k}} \hat{\mathbf{u}}(\mathbf{k}, t) \exp\left(i\mathbf{k} \cdot \mathbf{x}\right),$$

where $\mathbf{k} = (k_1, k_2, k_3)$, $k_i \in [-N_c/2, N_c/2 - 1]$ represent the 3D wave vectors and N_c is the number of collocation points. The incompressibility condition is used to eliminate the pressure term by introducing a transverse projection operator $\mathbb{P}_{\mathrm{i,j}}(\mathbf{k}) = \delta_{\mathrm{i,j}} - k_\mathrm{i} k_\mathrm{j}/k^2$ that projects the nonlinear term on a plane perpendicular to $\mathbf{k}$. The Fourier pseudo-spectral method relies on the computation of the linear terms in Fourier space and the nonlinear terms in real space, before transforming them back to Fourier space. Aliasing errors are removed using the standard 2/3-dealiasing rule, so that the maximum wave number in our simulations is $k_\mathrm{max} = N_c/3$. Both the

NS and the RNS dynamics are evolved in time using a second-order Runge-Kutta scheme. In our RNS numerics, the time-step was kept very small $dt = 7.5 \times 10^{-4}$, and this allowed us to have a very accurate conservation of the energy; errors are below 0.03 percent in our runs.

2. Initial data and forcing

Both the RNS and NS runs are initiated from the following Taylor-Green velocity field:

$$\begin{aligned} u_x &= u_0 \, \sin(x)\cos(y)\cos(z), \\ u_y &= -u_0 \, \cos(x)\sin(y)\cos(z), \\ u_z &= 0, \end{aligned}$$

where the coefficient u_0 sets the value of the initial energy.

In order to obtain statistically steady states, we inject energy in the system by using the Taylor-Green forcing:

$$\begin{aligned} f_x &= f_0 \sin(\tilde{k}_{\rm f} x)\cos(\tilde{k}_{\rm f} y)\cos(\tilde{k}_{\rm f} z), \\ f_y &= -f_0 \cos(\tilde{k}_{\rm f} x)\sin(\tilde{k}_{\rm f} y)\cos(\tilde{k}_{\rm f} z), \\ f_z &= 0, \end{aligned}$$

where f_0 and $\tilde{k}_{\rm f}$ are respectively the forcing amplitude and wave number. We write $k_{\rm f} := \sqrt{3}\tilde{k}_{\rm f}$ as the norm of the forcing wave vector $\mathbf{k}_{\rm f} = \left(\tilde{k}_{\rm f}, \tilde{k}_{\rm f}, \tilde{k}_{\rm f}\right)$.

As an aside, let us recall that the Taylor-Green flow has a vanishing total helicity, *e.g.* $\int_{\mathcal{D}} \mathbf{u}.(\nabla \times \mathbf{u}) = 0$.

3. Conventional definitions

We compute the isotropic energy spectrum as

$$E(k,t) := \frac{1}{2} \sum_{\substack{\mathbf{k}: \\ {\rm k}-\frac{1}{2} < |\mathbf{k}| \leq {\rm k}+\frac{1}{2}}} |\hat{\mathbf{u}}(\mathbf{k},t)|^2,$$

from which both the (total) energy $E := \sum_{k=1}^{k_{\max}} E(k,t)$ and the enstrophy $\Omega := \sum_{k=1}^{k_{\max}} k^2 E(k,t)$ are estimated.

The non-linear energy fluxes are defined through

$$\Pi(k,t) = \sum_{|\mathbf{k}| \geq k} T(\mathbf{k},t), \quad \text{where}$$

$$T(\mathbf{k},t) := \Re \left\{ \sum_{i,j=1,2,3} \hat{u}_i^\star[\mathbf{k},t] \; \mathbb{P}_{i,j}(\mathbf{k}) \left[\mathbf{u} \times \widehat{(\nabla \times \mathbf{u})} \right]_j [\mathbf{k},t] \right\}$$

represents the energy transfer function.

We finally define the forcing timescale as $\tau = \ell_{\rm f}/\sqrt{E_0}$, with E_0 denoting either the prescribed RNS energy or a suitable time-averaged NS energy. Please observe that in Fourier space, the reversible viscosity defined in Eq. (3), is computed as

$$\begin{aligned} &\nu_{\rm r}[\mathbf{u}] = \epsilon_{\rm inj}/\Omega, \quad \text{with } \Omega \text{ the enstrophy,} \\ &\text{and } \epsilon_{\rm inj} := \Re \left\{ \sum_{\substack{\mathbf{k}:|\mathbf{k}| \leq k_{\max} \\ i=1,2,3}} f_i(\mathbf{k},t) \cdot u_i^\star(\mathbf{k},t) \right\} \end{aligned} \tag{6}$$

representing the injected power due to the external forcing.

4. Parameters of the Simulations

In order to carry out a systematic investigation of the RNS system at fixed N_c and fixed forcing wave number $k_{\rm f} = \sqrt{3}$, we follow two protocols: (A) vary u_0 so that the runs have different E_0 for fixed f_0; (B) vary f_0 using the same prescribed initial velocity amplitude $u_0 = 1$ (in which case all the corresponding RNS runs have the same total energy). Our discussion is based on three sets of runs of resolution up to 128^3, the details and labels of which are summarized in Table I.

Set	N_c	$k_{\max}$	E_0	f_0
$\mathtt{A}_{64}$	64	21.3	From 0.06 to 2.2	0.13
$\mathtt{A}_{128}$	128	42.6	From 0.06 to 2.2	0.12
$\mathtt{B}_{128}$	128	42.6	0.125	From 0.012 to 0.12

TABLE I. The three sets of runs discussed in the present work.

B. Results

We now present our results from DNSs of the RNS system. We find that the time-averaged value of the enstrophy and reversible viscosity, as a function of the control parameter $\mathcal{R}_{\rm r}$, provides an insightful way to distinguish between the different statistical regimes of the RNS system. They serve as a relevant order parameter that clearly demarcates the phase diagram in two regions $\mathcal{R}_{\rm r} < \mathcal{R}_{\rm r}^- \simeq 2$ and $\mathcal{R}_{\rm r} > \mathcal{R}_{\rm r}^+ \simeq 3.2$, in accordance with the two asymptotic states $\mathcal{R}_{\rm r} \to 0$ and $\mathcal{R}_{\rm r} \to \infty$. We refer to the low-$\mathcal{R}_{\rm r}$ regime as a "warm" statistical states, as they are characterized by the presence of a partial thermalization at small length-scales and therefore are sensitive to the cutoff wave number $k_{\max}$. The high-$\mathcal{R}_{\rm r}$ regime is insensitive to this non-physical cutoff, and hence we refer to these states as being of "hydrodynamic" type. The range $\mathcal{R}_{\rm r}^- \leq \mathcal{R}_{\rm r} \leq \mathcal{R}_{\rm r}^+$ is a crossover region over which the mean value of the order parameter smoothly decreases from a finite positive values to a nearly vanishing one. Moreover, the vicinity of the critical point is characterized by the presence of strong fluctuations (bursts) in the enstrophy time series, whose origin in our understanding

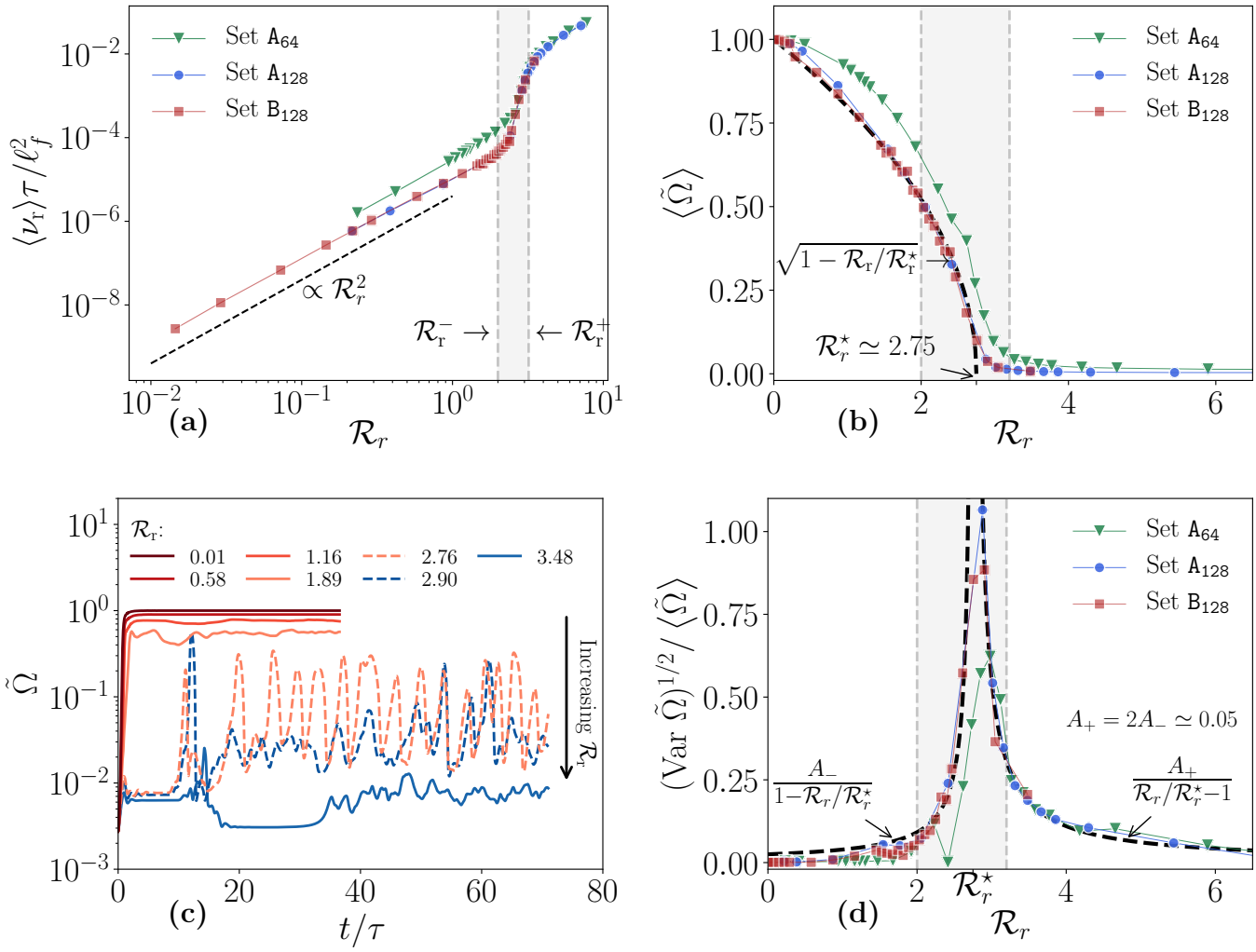

FIG. 2. **Signatures of the RNS phase transition.** (a) Time-averaged reversible viscosity ν_r vs. $\mathcal{R}_r$. Dotted lines represent the scaling $\nu_r \sim \mathcal{R}_r^2$, prescribed by the asymptotics $\mathcal{R}_r \to 0$ (see text for details). For $\mathcal{R}_r > \mathcal{R}_r^\star$, the reversible viscosity becomes independent of the cutoff $k_{\max}$. This signals that the regime is of hydrodynamic type. (b) Time-averaged normalized enstrophy $\widetilde{\Omega}$ vs. $\mathcal{R}_r$, exhibiting a smooth transition in the vicinity of $\mathcal{R}_r^\star \simeq 2.75$. $\widetilde{\Omega} \in [0, 1]$ acts as an *order parameter*. (c) Time series of the normalized enstrophy ($\widetilde{\Omega} := \Omega/\Omega_{eq}$) for representative values of the control parameter $\mathcal{R}_r$ from Set $\mathtt{B}_{128}$. (d) Time-variance of $\widetilde{\Omega}$ vs. $\mathcal{R}_r$ showing the enhancement of the enstrophy fluctuations near $\mathcal{R}_r \sim \mathcal{R}_r^\star$. In every figure, the grey-shaded area indicates a transition range delimited by $\mathcal{R}_r^- \simeq 2$ and $\mathcal{R}_r^+ \simeq 3.2$.

is linked to a non-trivial, ultra-violet multi-scale dynamics.

1. *Statistical states of the RNS system*

The enstrophy Ω is particularly sensitive to the onset of a thermalization at small length-scales (large wave numbers). For our purposes here, we find it convenient to normalize the enstrophy as $\widetilde{\Omega} := \Omega/\Omega_{\rm eq}$, where $\Omega_{\rm eq} = 3k_{\max}^2 E_0/5$ is the absolute equilibrium value (see Appendix A for details).

Note that the (non-signed) reversible viscosity, defined by Eq. (6), is also sensitive to the fluctuations at small length scales. Therefore, the time-averaged enstrophy and the reversible viscosity emerge as a natural choice for the order parameter, which allows us to distinguish between the different phases (statistical regimes) of the RNS system. In the asymptotic limit $\mathcal{R}_r \to 0$, i.e. in case of full thermalization, $\langle \nu_r \rangle \to 0$ and $\langle \tilde{\Omega} \rangle \to 1$, while the opposite limit $\mathcal{R}_r \to \infty$ (over-damped regime) corresponds to $\langle \nu_r \rangle \to \infty$ and $\langle \tilde{\Omega} \rangle \to 0$.

Figures 2 (a)-(b) show the values of $\langle \nu_r \rangle$ and $\langle \tilde{\Omega} \rangle$ as function of the control parameter $\mathcal{R}_r$, on which the crudely depicted "crossover region" of Fig. 1 between the small-$\mathcal{R}_r$ *thermalized* and the large-$\mathcal{R}_r$ *hydrodynamical* can be identified as the critical region in the close vicinity of $\mathcal{R}_r^\star = 2.75$.

This information can be refined by monitoring the dynamical behavior of the order parameters, rather than

their time-averaged values. To simplify the discussion, we choose to comment only on the fluctuations of the normalized enstrophy, which we show in Fig. 2(c) and (d). Specifically, Fig. 2 (c) displays the dynamical evolution $\tilde{\Omega}$ for representative values of $\mathcal{R}_\mathrm{r}$ corresponding to the RNS Set $\mathtt{B}_{128}$, while Fig. 2 (d) shows the relative amplitude of the fluctuations (standard-deviation of $\tilde{\Omega}$ relative to $\langle\tilde{\Omega}\rangle$) for all three sets of runs $\mathtt{A}_{64}$, $\mathtt{A}_{128}$ and $\mathtt{B}_{128}$ as a function of the control parameter $\mathcal{R}_\mathrm{r}$. The combined insight from both the averaged and dynamical behavior of $\tilde{\Omega}$ leads us to identify three sub-ranges of the control parameter $\mathcal{R}_\mathrm{r}$ that correspond to three different statistical regimes of the RNS system that we describe below.

a. The hydrodynamic range: $\mathcal{R}_\mathrm{r} > \mathcal{R}_\mathrm{r}^+ \simeq 3.2$.
In this range, the time-averaged reversible viscosities $\langle\nu_\mathrm{r}\rangle$ reach finite positive values. The data collapse observed in Fig. 2 (a) suggests that these values are described by an increasing function of $\mathcal{R}_\mathrm{r}$, independent of both the chosen protocol and the cutoff scale k_max. This feature is compatible with the normalized enstrophy $\langle\tilde{\Omega}\rangle$ being nearly vanishing and behaving as a decreasing function of $\mathcal{R}_\mathrm{r}$. Note that $\langle\tilde{\Omega}\rangle$ has some dependence on k_max, this is evident from the observation that its profile for set $\mathtt{A}_{64}$ in Fig. 2 (b) lies above those for sets $\mathtt{A}_{128}$ and $\mathtt{B}_{128}$.

Furthermore, the enstrophy time-series indicate that in this range of $\mathcal{R}_\mathrm{r}$, typical statistically steady states have low-amplitude enstrophy fluctuations. Empirical fits shown in Fig. 2 (d) reveal that the normalized temporal standard-deviations of the enstrophies are reasonably well described by $[\mathrm{Var}(\tilde{\Omega})]^{1/2} \simeq A_+\langle\tilde{\Omega}\rangle/(\mathcal{R}_\mathrm{r}/\mathcal{R}_\mathrm{r}^\star - 1)$, with $A_+ = 0.05$ and $\mathcal{R}_\mathrm{r}^\star = 2.75$, independent of k_max.

b. The warm range: $\mathcal{R}_\mathrm{r} < \mathcal{R}_\mathrm{r}^- \simeq 2$.
In this range of $\mathcal{R}_\mathrm{r}$, the order parameters show some dependence on k_max, as visible in Fig. 2 (a) and (b). For the reversible viscosity, this can be accounted for by using the Kubo dissipation theorem to estimate $\langle\epsilon_\mathrm{inj}\rangle \sim f_0^2\tau_\mathrm{eq}$ in the limit $\mathcal{R}_\mathrm{r} \to 0$. The timescale $\tau_\mathrm{eq} \sim \ell_\mathrm{f}E_0^{-1/2}$ is the *equilibrium* velocity correlation time at forcing length-scale, and is here prescribed by the statistics of the fully thermalized state of the truncated Euler flows [42, 43]. Combining this estimate with the definitions (5) and (6), and using Eq.(A2) found in Appendix A, one obtains

$$\langle\nu_\mathrm{r}\rangle \sim \frac{\mathcal{R}_\mathrm{r}^2 E_0^{3/2}}{\Omega_\mathrm{eq}\ell_\mathrm{f}} \propto \frac{\mathcal{R}_\mathrm{r}^2}{k_\mathrm{max}^2} \text{ as } \mathcal{R}_\mathrm{r} \to 0. \tag{7}$$

This asymptotics indeed accounts for the scaling behaviors observed in our numerics, which in fact is present in the entire warm range of $\mathcal{R}_\mathrm{r}$.

For the normalized enstrophy, the time-average $\langle\tilde{\Omega}\rangle$ observed for the higher resolved sets of runs prove to be very accurately fitted by the square-root profile $\langle\tilde{\Omega}\rangle = (1 - \mathcal{R}_\mathrm{r}/\mathcal{R}_\mathrm{r}^\star)^{1/2}$. The representative time-series of Fig. 2 (c) indicate that warm dynamics quickly reach steady states characterized by vanishing levels of fluctuations for the enstrophy. As a function of $\mathcal{R}_\mathrm{r}$, these are fairly well described by the fit $[\mathrm{Var}(\tilde{\Omega})]^{1/2} \simeq A_-\langle\tilde{\Omega}\rangle/(1 - \mathcal{R}_\mathrm{r}/\mathcal{R}_\mathrm{r}^\star)$, with $A_- = 0.025$.

At the present stage, the specific shapes of the fitting profiles should be considered as mere observations. Clearly, these fitting laws indicate a critical behavior, which is amenable to a mean-field treatment and is suggestive of a potential continuous phase transition. Yet, we postpone any further informed comments on the mean-field treatment up until § IV C 3, where similar behaviors will again appear but in a somewhat simplified setting, hence it is easier to gain insight.

c. The transition range: $\mathcal{R}_\mathrm{r}- < \mathcal{R}_\mathrm{r} < \mathcal{R}_\mathrm{r}^+$.
Within this narrow range of $\mathcal{R}_\mathrm{r}$, the order parameters sharply but *smoothly* transit between their warm and hydrodynamic behaviors: This precisely corresponds to the crossover region anticipated in Fig. 1. Let us observe that the critical value $\mathcal{R}_\mathrm{r}^\star \simeq 2.75$ previously obtained as a fitting parameter lies in this range. In fact, the mixed phase is essentially identified from the dynamical behavior of the enstrophy that becomes bursty, characterized by the appearance of successive peaks (*cf.* Fig. 2 (c)). This behavior is found to persist up to the maximal integration time that we considered. The bursty behavior implies that the enstrophy fluctuations get drastically enhanced with respect to their the mean enstrophy values when approaching $\mathcal{R}_\mathrm{r}^\star$ from either the warm or the hydrodynamic side, as is evident form Fig. 2 (d). At $\mathcal{R}_\mathrm{r} = \mathcal{R}_\mathrm{r}^\star$ for example, we observe $[\mathrm{Var}(\widetilde{\Omega})]^{1/2}/\langle\widetilde{\Omega}\rangle \sim 1$ for all three sets of runs, meaning that the temporal fluctuations are of the order of the time-averages. This behavior indicates finite-size effects and an associated potential continuous phase transition that occurs in the limit of infinite resolution, i.e. $k_\mathrm{max} \to \infty$.

2. *Spectral signatures of the RNS states*

Here we document the RNS energy spectra and fluxes observed in the different statistical regimes, with an aim to further characterize the phase diagram of the RNS system, without associating them with their NS counterpart or the equivalence conjecture, at least for now. Let us recall that the RNS dissipative term relies on an intrinsic direct dynamical coupling with the forcing length-scale. It is therefore highly non-local in Fourier space, in sharp contrast with the standard NS viscous damping, which is local in k-space. *A priori*, the spectral signatures of the different RNS states are not obvious; it is unclear whether we should at all expect the RNS system to even mimic the standard NS *phenomenology* for prescribed ranges of $\mathcal{R}_\mathrm{r}$.

a. Warm spectra vs. *hydrodynamic spectra.*
The analysis of § III B 1 revealed that within the warm and the hydrodynamic phases, RNS dynamics has non-equilibrium steady states characterized by very low enstrophy fluctuations. In both of these phases, it is

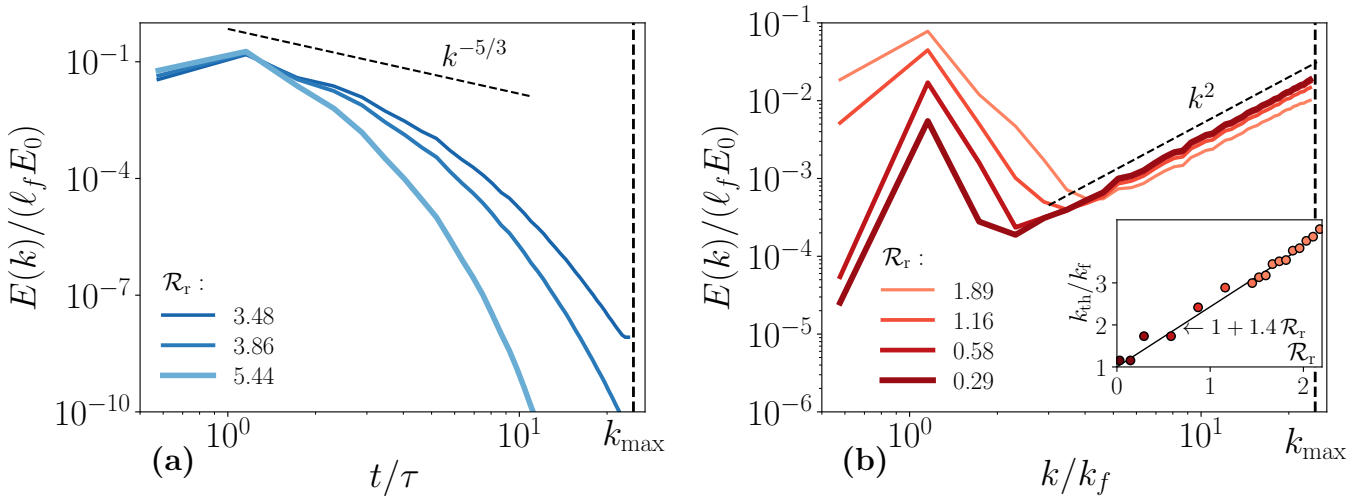

FIG. 3. **Warm spectra *vs.* hydrodynamic spectra.** Main panels show the suitably normalized time-averaged energy spectra observed in the RNS runs at $N_c = 128$ (from Set $\mathtt{B}_{128}$ and for $\mathcal{R}_r > 3.48$ from Set $\mathtt{A}_{128}$) for representative values of: (a) $\mathcal{R}_r > \mathcal{R}_r^+$ corresponding to the hydrodynamic regime; (b) $\mathcal{R}_r < \mathcal{R}_r^-$ corresponding to the warm regime. In the latter case, we observe an increasing range of wave numbers $k > k_{th}$ over which the spectra have Gibbsian scaling $E(k) \propto k^2$. k_{th} is the wave number at which $E(k)$ is minimal. The inset reveals a linear dependence of k_{th} on $\mathcal{R}_r$, and suggests $k_{th} \to k_f \simeq 1$ as $\mathcal{R}_r \to 0$.

therefore natural to focus on time-averaged quantities. We define the (stationary) energy spectrum as the time-average $E(k) := \langle E(k,t)\rangle$, where the bracket indicates an average over the total duration of the simulations. As shown in Fig. 3, both the warm and the hydrodynamical phase have distinct spectral signatures, which naturally links with the behavior of the order parameter studied in § III B 1.

In the hydrodynamical phase, $\mathcal{R}_r > \mathcal{R}_r^+$, the energy spectra have compact support in k-space, as shown in Fig. 3 (a). For $\mathcal{R}_r \gg R_+$, the supports is narrow, the spectra being contained within a small k-range around the forcing wave number. This means that the effective scale-by-scale damping mechanism generated from the reversible viscosity is large and dominates over the non-linear transfer, somewhat akin to a laminar regime. As $\mathcal{R}_r$ decreases down to $\mathcal{R}_r^+$, energy spreads towards the higher wave numbers $k > k_f$. The system is then in a non-trivial non-equilibrium steady-state, with non-zero flux of energy, and multi-scale statistics being essentially independent of k_{max}: This could be taken as a heuristic definition of a turbulent state [44]! From this qualitative point of view, the RNS statistics observed at $\mathcal{R}_r = 3.48 \gtrsim \mathcal{R}_r^+$ do indeed describe a turbulent motion.

At this stage, the rather modest resolution of our numerics compared to current state-of-the-art NS simulations precludes us from drawing any conclusion as to whether higher-resolved RNS simulations would indeed produce *fully developed turbulent statistics*, *e.g.*, akin to those found in numerical and experimental datasets related to extreme regimes of fluid motion [45, 46]. This issue is related to the equivalence conjecture and we will discuss it in details in § V A, in connection with our discussion on turbulent limits.

In the warm phase, here identified as $\mathcal{R}_r < \mathcal{R}_r- \simeq 2$, the spectra are contaminated by the finite cutoff, as shown in Fig. 3 (b). Specifically, they resemble some of the transients commonly observed in numerical simulations of the truncated Euler dynamics [37, 38, 47], in the sense that a seemingly infra-red traditional hydrodynamic scaling at small k coexists with a near equilibrium ultra-violet power law scaling, that is $E(k) \sim k^\alpha$, where α progressively increases towards the Gibbs exponent $\alpha = 2$ as $\mathcal{R}_r$ decreases towards 0. The separation between the two regions is identified in terms of a thermal wave number k_{th}, defined as the local minimum of the energy profile. The inset of Fig. 3 (b) shows that as $\mathcal{R}_r \to 0$, k_{th} decreases linearly towards a value close to the forcing scale $k_{th} = \sqrt{3}$, *e.g.* close to the smallest wavenumber $k_0 = 1$. This is compatible with the fact that at $\mathcal{R}_r = 0$, the RNS steady state in fact corresponds to a fully thermalized *equilibrium* state of the truncated Euler equations, as explained in § II B. Naturally, the approximate ultra-violet thermalization at $k > k_{th}$ accounts for the fact that the warm phase has a non-vanishing order parameter $\langle\tilde{\Omega}\rangle$, as indeed observed in Fig. 2, and explained with more technical details in Appendix A.

b. Energy spectra in the transition range.

In the transition region, as evidenced by the violent fluctuations observed in the enstrophy time series, it is unclear whether the system genuinely reaches a steady state. It proves therefore more instructive to comment on

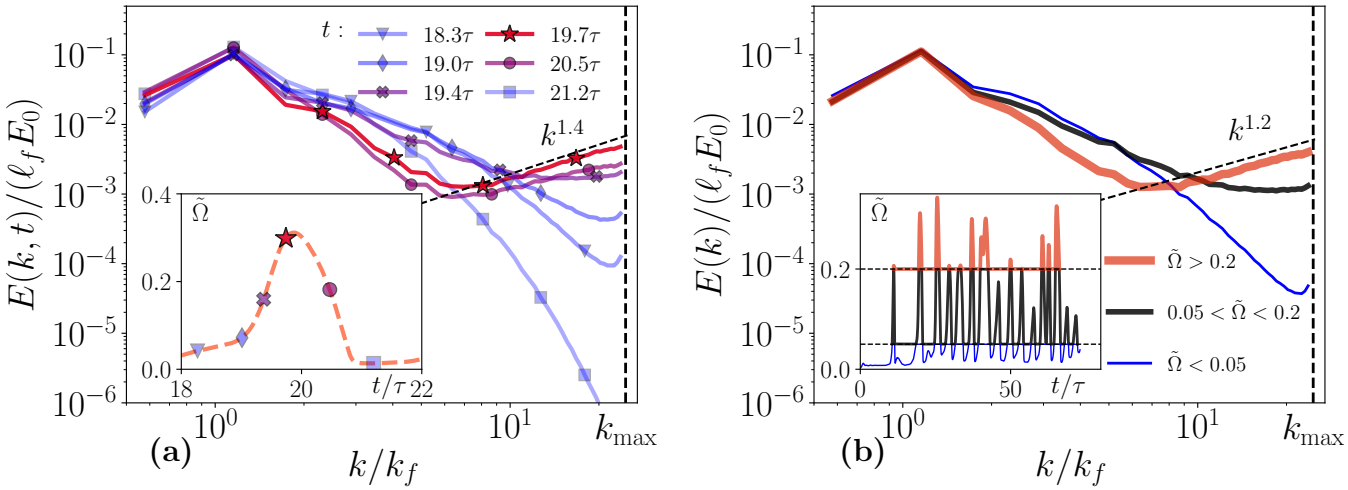

FIG. 4. **Spectral multi-stability in the transition region, $\mathcal{R}_r^- < \mathcal{R}_r < \mathcal{R}_r^+$.** Panel (a) shows duly normalized *instantaneous* energy spectra from the RNS run $\mathcal{R}_r = 2.76$ of Set $\mathtt{B}_{128}$, at selected times, so as to trace one of the enstrophy burst shown in Fig. 2 (c). Inset shows the zoom of the enstrophy burst in the time series. Panel (b) displays time-averages of the energy spectra, conditioned on specific magnitudes of the normalized enstrophy, as specified by the inset.

the dynamics of the instantaneous energy spectra $E(k,t)$, rather than on their time-averaged values. In fact, the peaks observed in Fig. 2 (c) clearly relates to oscillations of the ultra-violet behavior near $k_{\max}$. We illustrate this by using the RNS run of set $\mathtt{B}_{128}$, corresponding to $\mathcal{R}_r = 2.76$, a value close to the identified critical point $\mathcal{R}_r^\star = 2.75$ at which the fluctuations are the most enhanced. Fig. 4(a) reports the dynamical evolution of the energy spectra $E(k,t)$ on a short time interval $18\tau < t < 22\tau$, over which the normalized enstrophy abruptly varies from $\tilde{\Omega} \simeq 0.03$ at $t \simeq 18.3\tau$ to $\tilde{\Omega} \simeq 0.3$ at $t \simeq 19.7\tau$ back to $\tilde{\Omega} \simeq 0.01$ at $t = 21.2\tau$. Over this time interval, the infra-red energy spectra near the forcing length-scale remains essentially unchanged, but the ultra-violet profile drastically varies. It transits between being exponentially damped and being algebraic, with time-dependent scaling $E(k,t) \propto k^{\alpha(t)}$, over a scaling range whose size increases with the exponent α.

As the enstrophy increases in time towards its peak value, the exponent $\alpha(t)$ itself switches from negative to positive values, and the scaling-range develops on a gradually increasing range. Let us observe, that the maximum value reached by the scaling exponent is 1.4 and not 2, as would be expected if the system was partially thermalized.

We know that the enstrophy is particularly sensitive to the dynamical evolution of small length-scales. This is further illustrated in Fig. 4, where time-averages of the energy spectra conditioned on prescribed enstrophy values are indeed observed to yield very different ultra-violet scaling ranges. For example, conditioning on $\tilde{\Omega} < 0.05$ yields a close-to-hydrodynamic type spectrum, while conditioning on the highest values $\tilde{\Omega} > 0.2$ produce ultra-violet scaling reminiscent of a warm one. Again, a closer inspection reveals that the relevant scaling exponent is only 1.2 and not 2.

This implies that while a finite $k_{\max}$ indeed produces non-zero values for the order parameter $\langle\tilde{\Omega}\rangle$, the latter should vanish in the limit $k_{\max} \to \infty$. This naturally hints that the crossover range should disappear in this limit. This would imply $\mathcal{R}_r^- = \mathcal{R}_r^+ = \mathcal{R}_r^\star$ asymptotically, and strongly suggests that the transition between the warm states and the hydrodynamics states becomes a genuine continuous phase transition in the limit $k_{\max} \to \infty$.

c. *Energy fluxes.*

In order to conclude our overview of the RNS states, let us briefly comment on the RNS energy fluxes, whose profiles for set $\mathtt{B}_{128}$ are shown in Fig. 5, wherein they have been normalized by the time-averaged injected power $\langle\epsilon_{\rm inj}\rangle$. The transition from the hydrodynamic to the warm regime is reflected by the k-space profiles of the time-averaged fluxes $\Pi(k) := \langle\Pi(k,t)\rangle$, as shown in Fig. 5 (a).

The flux profiles observed within the hydrodynamic range clearly mirror the energy spectra observations of § III B 2 a. For large $\mathcal{R}_r > \mathcal{R}_r^+$, fluxes are indeed non-zero only in a small range of wave numbers $k \gtrsim k_f$. As $\mathcal{R}_r$ decreases down to $\mathcal{R}_r^+$, the spectral extension of the fluxes increases. For example, at $\mathcal{R}_r \approx 3.48$, where the energy spectra suggest that RNS dynamics is multi-scale, we observe an energy flux that is significant up to $k \approx 10\,k_f$: This is in qualitative agreement with standard NS phenomenology at low Reynolds number. In particular, it is not evident from the fluxes that the

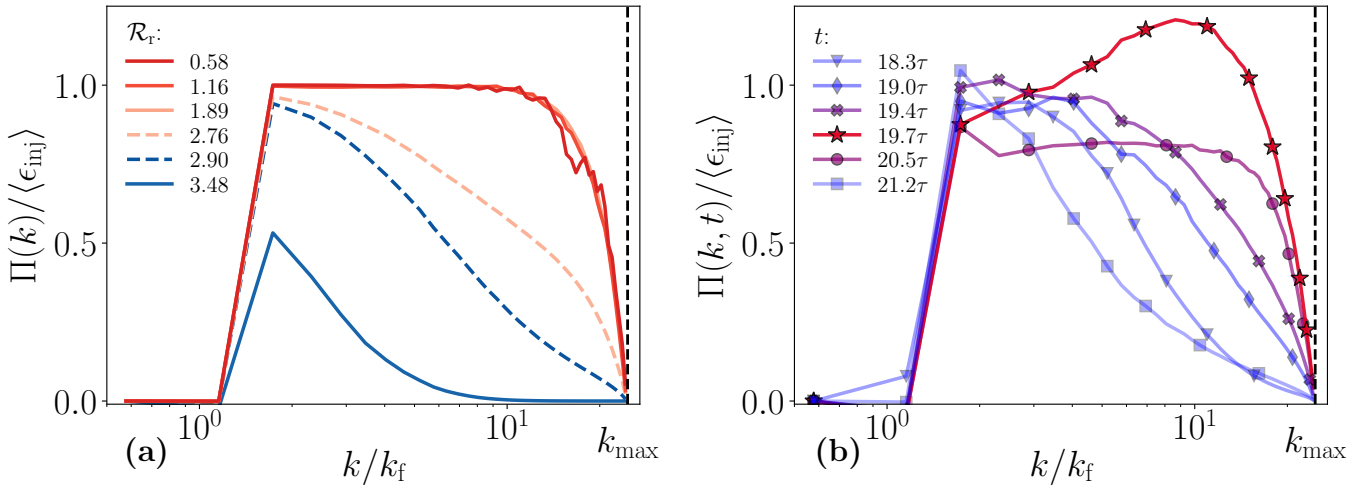

FIG. 5. **RNS Energy fluxes.** Panels show the k-space profile of the energy fluxes $\Pi(k)$ normalized by the time-averaged injected power $\langle\epsilon\rangle_{\rm inj}$, computed from Set $\mathtt{B}_{128}$: (a) averaged over time for values of $\mathcal{R}_r$ representing different RNS regimes; (b) for the $\mathcal{R}_r = 2.76$ run within the crossover region, at the same specific times considered in Fig. 4 (a) and tracing the enstrophy burst shown in the corresponding inset.

reversible dissipation is defined as a non-local operator in k-space.

Within the warm range $\mathcal{R}_r < \mathcal{R}_r^-$, the fluxes follow a universal profile, that is seemingly independent of the specific value of $\mathcal{R}_r$, as indicated by the data collapse observed for $0.58 \lesssim \mathcal{R}_r \lesssim 1.89$. This is a clear signature of the warm statistical regime, but is counter-intuitive.

On the one hand, except for their abrupt decay to zero at the ultra-violet end, the fluxes are mostly constant over the entire k-range above the forcing scale, *e.g.* here $2k_f \lesssim k \lesssim 20k_f$: This signals an out-of-equilibrium state, that should imply Kolmogorov-scaling for the spectra. On the other hand, the corresponding energy spectra do not show this Kolmogorov spectra. Instead, Fig. 3 (b) indicates close-to-equilibrium statistics, with a "distance" towards full thermalization monitored by the scale $k_{\rm th}$ becoming arbitrarily close to 1 as $\mathcal{R}_r \to 0$. This gradual convergence towards the equipartition state is not reflected by the flux profiles.

A qualitative explanation could be that the energy flux is an integrated quantity (see § III A 3). Hence, if the range $k > k_{\rm th}$ is indeed nearly thermalized as prescribed by the equipartition statistics, then they do not contribute to the flux. An impatient and puzzled reader can however jump to the discussion of Eq. (16) at the end of § IV C 1 to find that this kind of profile is in fact fully compatible with near-equilibrium and partially thermalized statistics.

As an aside, let us point out that in the "warmest range" $\mathcal{R}_r \lesssim 0.5$, not shown here, $\Pi(k)$ begins to fluctuate wildly from the ultra-violet end. The amplitude of the normalized fluctuation grows with decreasing $\mathcal{R}_r$ and destroys the plateau behavior. The amplitude of the non-normalized $\Pi(k)$ however correctly goes to zero and this is compatible with the truncated Euler limit with $E(k) \sim k^2$ across the full k-range.

Within the transition range $\mathcal{R}_r^- < \mathcal{R}_r < \mathcal{R}_r^+$, Fig. 5 indicates that the large enstrophy fluctuations reflect the fact that the instantaneous fluxes $\Pi(k,t)$ oscillate in time between a narrow-band hydrodynamic-type profile (at $t = 21.2\tau$ for example) and a multitude of full-band profiles, which for instance include the constant profile at $t = 20.5\tau$ or the non-monotonic bumpy profile peaked at $k \simeq 10k_f$ in the vicinity of $k_{\rm max}$ at $t = 19.7\tau$, and corresponds to the local maximum monitored in the enstrophy time series.

IV. INSIGHTS FROM A REVERSIBLE LEITH-TYPE TOY MODEL

Our numerical analysis so far shows that the RNS system undergoes a continuous phase transition at the critical point $\mathcal{R}_r^\star$, whereby steady RNS solutions transit from being *hydrodynamic* to being *warm*, in the sense that their ultra-violet statistical features become affected by truncation scale and eventually thermalize. The smoothness of the transition is however a necessary consequence of our RNS runs having a finite resolution. Even though the behavior of the order-parameters (see Fig. 2) appears to be consistent with the phenomenology a second-order transition occurring at $\mathcal{R}_r^\star \simeq 2.75$, the numerical evidence is only suggestive. Our runs have finite resolutions, and this in principle precludes true divergence of any first derivative of the control parameter at the candidate critical point. For a

similar reason, while we argued that the RNS equations at $\mathcal{R}_{\rm r} \gtrsim \mathcal{R}_{\rm r}{}^{\star}$ produce multi-scale steady states that fit the heuristic definition of "turbulence"; we are well aware that such a statement is only qualitative, due to the modest resolutions of our RNS runs. Consequently, it cannot provide a firm assessment regarding the validity of the equivalence conjecture. This is the reason why no quantitative comparison with NS runs have been commented on so far.

Even though higher resolutions simulations are desirable, nevertheless, further insights about the nature of the transition can be obtained at a smaller numerical cost from a simplified non-linear diffusion spectral model of turbulence, namely a modified Leith model of turbulent cascade [48], which mimics the statistical properties of the RNS system. This model is easier to analyze as its steady solutions can determined semi-analytically [36, 49–51]. Note that the terminology "warm solutions" used in the present paper is borrowed from the concept of "warm cascades" introduced in Ref. [36], which is a stationary solution of the inviscid Leith model that exhibits simultaneously the Kolmogorov infra-red scaling and thermalized Gibbsian ultra-violet statistics.

Our analysis of the reversible Leith model suggests that its steady solutions indeed undergo a second-order phase transition, which separates the hydrodynamic scaling from the warm solutions. The transition is controlled by a parameter $\mathcal{R}_L$, similar to the control parameter $\mathcal{R}_{\rm r}$ of the RNS system, and the phase diagram at finite $k_{\max}$ is qualitatively similar to the one inferred from the RNS simulations. The parameter $1/k_{\max}$ plays the role of a symmetry breaking parameter, which is reminiscent of the magnetic field in the Ising model. In the limit $k_{\max} \to \infty$, this system undergoes a genuine continuous phase transition, at which a suitably defined susceptibility diverges. Moreover, we find that the statistical features of this phase transition can be captured by constructing a mean-field Landau free energy. We argue that this picture extends to the RNS system and has practical implications for the equivalence conjecture.

A. Description of the Reversible Leith model

The inviscid Leith model [36] consists in approximating dynamics of the energy spectrum in k-space using a well-chosen second-order non-linear diffusive operator. We here combine this non-linear evolution for the energy profile $E(k,t)$ with a thermostat. The Reversible Leith (RL) dynamics is then simply described by

$$\begin{aligned} &\frac{\partial E(k,t)}{\partial t} = -\frac{\partial \pi(k,t)}{\partial k} - \nu_L k^2 E(k,t), \\ &\text{where} \quad \pi(k,t) = -C k^{11/2} E^{1/2}(k,t) \frac{\partial}{\partial k}\Big[\frac{E(k,t)}{k^2}\Big] \end{aligned} \tag{8}$$

represents an energy flux and C is a dimensional constant that can be set to 1 for the present purpose. The wave numbers k range from prescribed k_0 to the truncation wave number $k_{\max}$. In analogy with the RNS system, we interpret the parameter ν_L as a reversible viscosity that guarantees the conservation of the total energy

$$\int_{k_0}^{k_{\max}} E(k,t)\, dk = E_0 \ \ \text{(prescribed)}. \tag{9}$$

We seek to characterize the non-equilibrium steady energy spectra $E(k)$ and the associated flux $\pi(k)$, generated by the RL dynamics (8), when the following fluxes are prescribed at the boundaries :

$$\pi(k_0) = \epsilon_0 \ \text{ and } \ \pi(k_{max}) = 0. \tag{10}$$

Combining the stationarity condition

$$-\frac{\partial \pi(k)}{\partial k} = \nu_L k^2 E(k) \tag{11}$$

with the boundary flux conditions Eq. (10), the reversible viscosity can be explicitly tied to the stationary energy profile $E(k)$ as

$$\nu_L = \frac{\epsilon_0}{\int_{k_0}^{k_{\max}} k^2 E(k)\, dk}. \tag{12}$$

The independent parameters that control the behavior of the steady energy profile are k_0, $k_{\max}$, E_0, together with the infra-red boundary flux ϵ_0. Letting $k_{\max} \to \infty$ and $\nu_L \to 0$ allows the possibility of non-vanishing constant flux solutions, characterized by the Kolmogorov scaling $E(k) \sim k^{-5/3}$. Such Kolmogorov solutions have finite capacity spectra, namely $\int_{k_0}^{+\infty} E(k)\, dk < \infty$. In other words, the value of the total energy is independent of $k_{\max}$ when $k_{\max} \to \infty$; therefore, it is natural to define a dimensionless number independent of $k_{\max}$, as

$$\mathcal{R}_{\rm L} = \epsilon_0^{2/3} \ell_0^{2/3} {E_0}^{-1}, \text{ with } \ell_0 = 2\pi/k_0. \tag{13}$$

The factor 2π entering the definition of the small scale ℓ_0 is purely cosmetic. Although it is defined in terms of a flux rather than in terms of a forcing intensity, the dimensionless number $\mathcal{R}_{\rm L}$ is the Leith analogue of our previously defined $\mathcal{R}_{\rm r}$ for the RNS system. It is the ratio of the injected energy at scale ℓ_0 and the total energy present in the system.

B. Construction of RL steady solutions

1. *Grebenev parametrization*

In order to construct steady solutions for the RL dynamics without resorting to direct numerical simulations of Eq.(8), we resort to the general strategy described in [51]. The idea is to introduce a suitable parametrization (hereafter referred to as the "Grebenev parametrization") of the energy profile that transforms

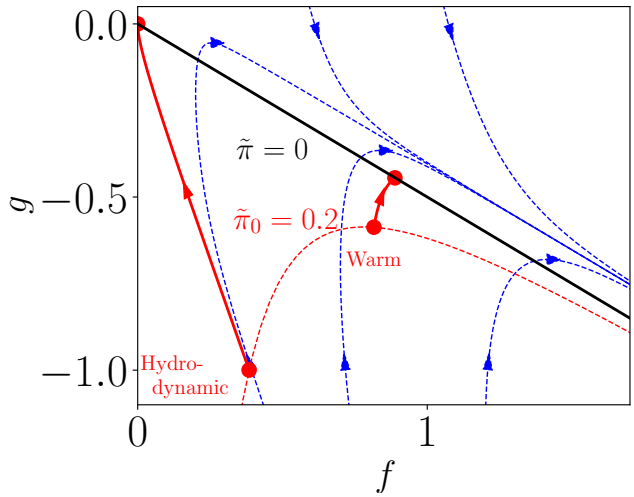

FIG. 6. Phase portrait of the dynamical system Eq. (15) obtained from the Grebenev parametrization of the Leith stationary profiles. Blue lines represent orbits and solid red lines are two examples of parameterizing trajectories with the same non-normalized infra-red flux $\tilde{\pi}_0$. A warm solution with vanishing end-point energy flux follows a typical orbit up until the black line, while a scaling solution follows the single orbit that ends at $(0,0)$. Note that the two represented solutions have different $k_{\max}$.

.

the stationarity condition Eq. (11) into an autonomous bi-dimensional dynamical system.

The specific form of the Grebenev parametrization is not particularly intuitive, but proves to be highly efficient. It consists in describing the steady energy profile using the change of variables $k, E(k), E'(k) \to \tau, f(\tau), g(\tau)$ defined through

$$\tau := \nu_L^{1/2} \int_{k_0}^{k} d\kappa \, (\kappa E(\kappa))^{-1/2}, \qquad (14)$$
$$f(\tau) := \left(E(k)\nu_L^{-1}k^{-1}\right)^{1/2}, \text{ and } g(\tau) := f'/f - f.$$

In terms of these variables, the stationary condition (11) transforms into the dynamical system

$$\begin{aligned} f'(\tau) &= f(f+g), \\ g'(\tau) &= -2(f+g)^2 - \frac{7}{2}f(f+g) + 2f^2 + \frac{1}{2}f. \end{aligned} \qquad (15)$$

This system admits a stable fixed point $(0,0)$ and its phase portrait is shown in Fig. 6.

2. *Practical use of the Grebenev parametrization*

For a practical use of the Grebenev parametrization (14), it is convenient to work with the non-normalized energy spectra and fluxes, respectively defined as

$$\tilde{E}(k) := E(k)/\nu_L^2 = kf^2(\tau),$$
$$\text{and } \tilde{\pi}(k) := -\pi(k)/\nu_L^3 = k^4 f^2(f+2g).$$

For given k_0 and $k_{\max}$, we can then obtain RL steady solutions by integrating the system Eq. (15) from $\tau = 0$ with initial conditions f_0, g_0 until time $\tau_{\max}$, implicitly defined from Eq. (14) as $\tau_{\max} = \int_{k_0}^{k_{\max}} dk/(kf(\tau))$. To construct the admissible solutions that satisfy the boundary conditions of type Eq. (10), we proceed in the following manner:

1. Pick an initial value $\tilde{\pi}_0$ for the non-normalized flux at point k_0. Initial admissible (f_0, g_0) are then such that $\tilde{\pi}_0 = k_0^4 f_0^2 (f_0 + 2g_0)$.
2. Find (f_0, g_0), such that $f(\tau_{\max}|f_0, g_0) + 2g(\tau_{max}|f_0, g_0) = 0$. This ensures that $\pi(k_{\max}) = 0$ (up to some prescribed threshold).
3. Compute $\nu_L = \left(\int_{k_0}^{k_{\max}} dk \tilde{E}(k)\right)^{-1/2}$.
4. Deduce $\epsilon_0 = \nu_L^3 \tilde{\pi}_0$.

The resulting solution is a steady-solution for the RL dynamics, with infra-red flux ϵ_0. Examples of trajectories in the (f, g)-plane that parametrize either a hydrodynamic solution or a warm solution are represented in Fig. 6.

C. Transition between Warm and Hydrodynamical steady states

1. *Qualitative overview*

Using the Grebenev parametrization, we generate the RL steady energy and flux profiles for fixed $k_0 = 10^{-2}$, and various $k_{\max}$ ranging from $5k_0$ to $1000k_0$. For each pair $(k_0, k_{\max})$, we typically vary the non-normalized infra-red flux $\tilde{\pi}_0$ from 10^{-10} to 10^{10}. The total energy E_0 is set to unity. We observe that at fixed k_0 and $k_{\max}$, the steady RL solutions are uniquely determined by the value of the infrared-boundary flux ϵ_0. The corresponding values of the reversible viscosity are then uniquely determined.

Figure 7 provides a qualitative overview of the various statistical regimes of the RL system that are generated by using our algorithm, which depend on the values of $\mathcal{R}_{\mathrm{L}}$. To provide an illustrative example, we take $k_0 = 10^{-2}$ and $k_{max} = 1$. In Fig. 7 (a) and (b) we show the energy spectra and the corresponding energy fluxes, respectively, for various values of $\mathcal{R}_{\mathrm{L}}$. It is clear that the RL dynamics exhibits a transition similar to the one observed for the RNS system. Moreover, RL system refines the overall picture, as it allows us to have a broader range of scales and also because of its intrinsic simplicity compared to the RNS system.

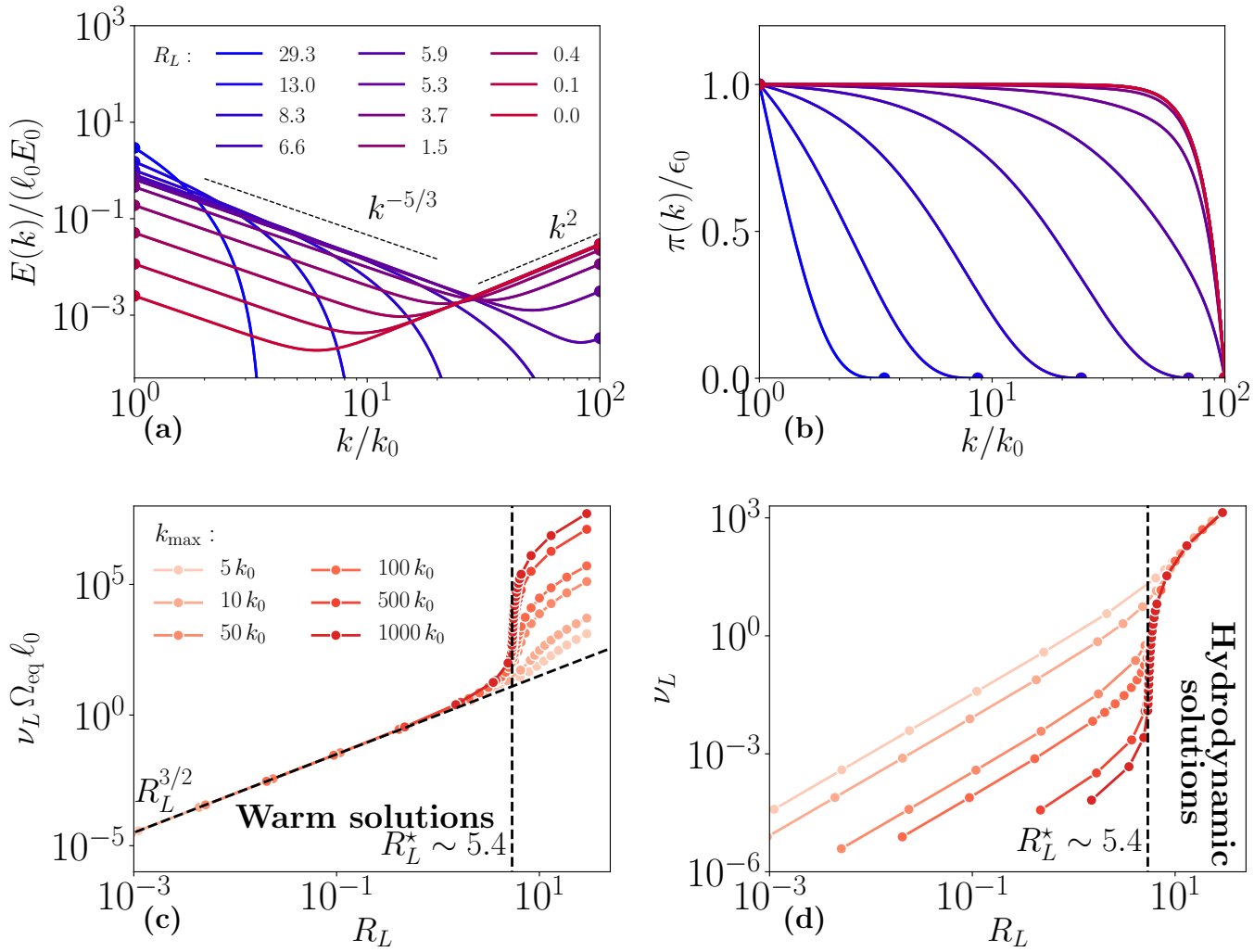

FIG. 7. **Transition between warm and hydrodynamic states in the Leith model**. Top panel shows the evolution of the steady profiles of (a) energy spectra and (b) energy fluxes, for fixed values of $k_0 = 1/\ell_0 = 10^{-2}$ and $k_{\max} = 1$. Above $\mathcal{R}_{\rm L}^\star \sim 5.4$, the energy spectra have compact support and exhibit inertial range Kolmogorov scaling. Below $\mathcal{R}_{\rm L}^\star$, both Kolmogorov and equipartition scalings coexist: This is the warm regime. The corresponding energy fluxes are then constant throughout the scales and their normalized profile become independent of $\mathcal{R}_{\rm L}$. Bottom panel shows the behavior of the RL viscosity as a function of $\mathcal{R}_{\rm L}$ for different values of $k_{\max}$: (c) with a suitable normalization illustrating the warm asymptotics $\nu_L \sim R_L^{3/2}/\Omega_{\rm eq}\ell_0$; (d) without normalization, illustrating universality of the hydrodynamic regime with respect to $k_{\max}$.

At large values of $\mathcal{R}_{\rm L}$, the energy spectrum has compact support in k-space and is therefore of hydrodynamic type. For $\mathcal{R}_{\rm L} \simeq 29.3$, the highest values considered, the energy spectrum $E(k)$ lacks any scaling region and is concentrated around the smallest wave number k_0. This is also true for the energy flux. This corresponds to an overdamped regime, wherein the non-linear terms are unable to transfer the injected energy to smaller length-scales.

When $\mathcal{R}_{\rm L}$ is decreased ($\mathcal{R}_{\rm L} \gtrsim 5.3$), the solutions develop an inertial range with Kolmogorov energy spectra $E(k) \sim k^{-5/3}$, followed by a fast exponential decay to zero at high wave numbers; for $\mathcal{R}_{\rm L}$ Kolmogorov scaling is present almost over the entire range of wave numbers. This is accompanied by the associated energy flux becoming essentially constant over an increasing range of wave numbers. Let us remark that the development of a pure Kolmogorov scaling range in this hydrodynamic regime is less obvious than it would seem at first thought: In particular, this is in contrast with the anomalous scaling solutions that typically appear in freely decaying infinite-range Leith models, whose infra-red scaling exponents are known to be systematically larger than the constant-flux exponents [36, 50].

At $\mathcal{R}_{\rm L} \sim 5.3$ the statistical character of the RL dynamics sharply changes to that of a warm regime. For $0 < \mathcal{R}_{\rm L} \lesssim 1.5$, both the Kolmogorov scaling $E(k) \sim k^{-5/3}$ and the thermalization scaling $E(k) \sim k^2$ coexist on the energy spectrum. Note that as $\mathcal{R}_{\rm L}$ de-

creases down to 0, the thermalization gradually invades the entire available wave number range. The associated warm energy fluxes are non-vanishing and mostly constant, irrespective of the size of the thermalized wave number region on the energy spectrum. This exactly mimics the counter-intuitive behavior observed in the RNS system (see Fig. 5) [52].

In the Leith case, this puzzling but robust signature of the warm regime can however be accounted for. Let us first note that at fixed k_0 and E_0, the definition of $\mathcal{R}_\mathrm{L}$ implies that $\mathcal{R}_\mathrm{L} \to 0$ as $\epsilon_0 \to 0$. We caution that the apparent constant nature of the *normalized* energy fluxes in Fig. 7 (b) in the $\mathcal{R}_\mathrm{L} \to 0$ limit should not misguide the reader into thinking that the flux is non-vanishing in the limit $\mathcal{R}_\mathrm{L} \to 0$. We emphasize that this is not the case here; this non-anomalous feature is in due agreement with the statement that $\mathcal{R}_\mathrm{L} \to 0$ corresponds to fully thermalized statistics. We also remark that in the limit $\mathcal{R}_\mathrm{L} \to 0$, the reversible viscosity $\nu_L \to 0$, as is clear from Figs. 7 (c) and (d).

The fact that the flux is constant across the scales is then a direct consequence of the stationarity condition Eq. (11), which reduces to $\partial_k \pi(k) = 0$ in the limit of vanishing reversible viscosity ν_L. Solving for the corresponding energy profiles up to an overall normalization constant, we obtain

$$E(k) \propto \left(5\left(\frac{k}{k_\mathrm{th}}\right)^3 + 6\left(\frac{k}{k_\mathrm{th}}\right)^{-5/2}\right)^{2/3}, \qquad (16)$$

where k_th is the wavenumber at which $E(k)$ reaches its minimum; note that k_th depends on the initial conditions (ϵ_0, k_0). It is readily checked that $E(k) \sim k^{-5/3}$ for $k \ll k_\mathrm{th}$ and $E(k) \sim k^2$ for $k \gg k_\mathrm{th}$: Eq. (16) provides an explicit example of a RL warm solution! There is therefore no contradiction in the simultaneous occurrence of a constant flux and a warm spectrum. Although the diffusion approximation is not valid in the RNS system, we believe that the property will carry through the RNS equations. Even though counter-intuitive, the constant fluxes observed at low $\mathcal{R}_\mathrm{r}$ in Fig. 5 are fully compatible with the statement that the RNS statistics are warm in that regime.

2. *Reversible viscosity and the continuous phase transition*

The above description of the statistical regimes of the RL dynamics, at fixed values of (k_0, k_max), holds in general and is mostly insensitive to the specific choice of k_max, provided that k_max/k_0 is sufficiently large. This can be directly inferred by monitoring the behavior of the reversible viscosity as a function of $\mathcal{R}_\mathrm{L}$, which we show in Fig. 7 (c) and (d) for different values of k_max. The partitioning between the warm and the hydrodynamic regimes is clear and the transition value to a first order approximation is independent of k_max. The sharpening of the reversible viscosity profile $\partial_{\mathcal{R}_\mathrm{L}} \nu_L|_{\mathcal{R}_\mathrm{L}=\mathcal{R}_\mathrm{L}^\star} \to \infty$ in the thermodynamic limit $k_\mathrm{max} \to \infty$ suggests that the system undergoes a genuine phase transition at $\mathcal{R}_\mathrm{L} = \mathcal{R}_\mathrm{L}^\star \simeq 5.4$. The observed continuity of the reversible viscosity at $\mathcal{R}_\mathrm{L} \approx \mathcal{R}_\mathrm{L}^\star$ indicates the phase transition is continuous. The warm and hydrodynamic regimes can therefore be identified as genuine *thermodynamic phases*.

In the warm phase $\mathcal{R}_\mathrm{L} < \mathcal{R}_\mathrm{L}^\star$, the scaling behavior of ν_L for finite k_max, is easily deduced from the definitions Eq. (12) and Eq. (13). As $\mathcal{R}_\mathrm{L} \to 0$, we indeed obtain $\nu_L \sim \epsilon_0/\Omega_\mathrm{eq} \sim (E_0\mathcal{R}_\mathrm{L})^{3/2}/(\ell_0\Omega_\mathrm{eq})$, with Ω_eq denoting the value of the enstrophy when the energy spectrum is fully thermalized and $\propto k^2$. Fig. 7 (c) shows that the scaling in fact extends up until $\mathcal{R}_\mathrm{L} \overset{<}{\to} \mathcal{R}_\mathrm{L}^\star$. Please observe that the dependence of ν_L on the cutoff parameter through $\Omega_\mathrm{eq} \propto k_\mathrm{max}^2$ signals partial thermalization of small length-scales, and implies that $\nu_L \to 0$ as $k_\mathrm{max} \to \infty$.

In the hydrodynamic phase, the reversible viscosity is independent of k_max (see Fig. 7 (d)). This reflects the fact that the statistics observed at finite $\nu_L > 0$ are mostly independent of k_max as $k_\mathrm{max} \to \infty$. The continuity of the reversible viscosity implies $\nu_L \to 0$ as $\mathcal{R}_\mathrm{L} \overset{>}{\to} \mathcal{R}_\mathrm{L}^\star$.

3. *Mean-field Landau free energy*

The interpretation of the RL "Warm/Hydrodynamic" transition in terms of a continuous phase transition can in fact be further substantiated and described in terms of a heuristic Landau theory (see, *e.g.*, [53]) involving the parameters

$$\begin{aligned} &r := \mathcal{R}_\mathrm{L}/\mathcal{R}_\mathrm{L}^\star - 1 \quad (\text{"reduced temperature"}),\\ &\mu := \tilde{\Omega}^{1/2} = (\Omega/\Omega_\mathrm{eq})^{1/2} \quad (\text{"magnetization"}),\\ &h := k_0/k_\mathrm{max} \quad (\text{"magnetic field"}). \end{aligned} \qquad (17)$$

Our choice of parameters is essentially data-driven and motivated by a succession of empirical trials. Note that the order parameter μ can as well be defined using the reversible viscosity as $\mu \propto \nu_L^{-1/2}$. This hydrodynamic analogue of magnetization is sensitive to ultra-violet thermalization and takes value 1 at $\mathcal{R}_\mathrm{L} = 0$. In the hydrodynamic phase, it is non vanishing for finite k_max, but converges to 0 at $\mathcal{R}_\mathrm{L}^\star$ as $k_\mathrm{max} \to \infty$. This feature together with the fact that the transition is smooth (absence of singular behavior) for finite values of k_max is the main indication as to why (one over) k_max may be suitable as a smoothing symmetry breaking parameter. Let us now consider the mean-field Landau free energy

$$\begin{aligned} &\phi_L(\mu, h, r) := -3h\mu + \frac{1}{2}r^2\mu^2 + \frac{1}{4}\mu^4,\\ &\text{defined for } \mu \geq 0, h \geq 0, r \geq -1. \end{aligned} \qquad (18)$$

In spite of its simplicity, Fig. 8 reveals that the mean-field free energy ϕ_L captures the essential signatures of

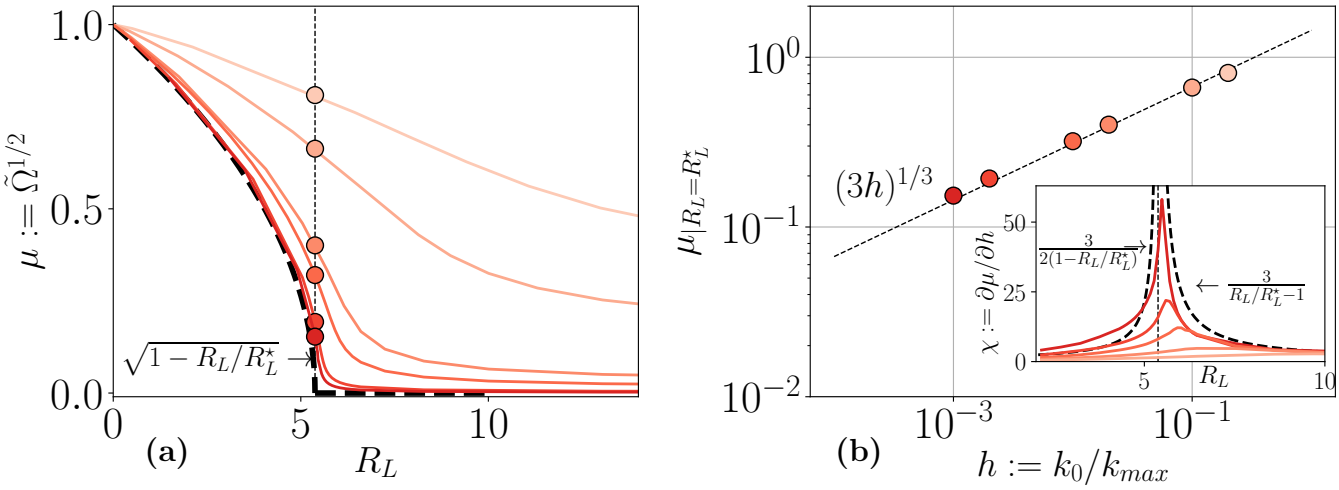

FIG. 8. **Mean-field behavior of the RL transition**. Panel (a) shows the spontaneous RL magnetization μ as a function of $\mathcal{R}_\mathrm{r}$ for $h = k_0/k_\mathrm{max}$ ranging from 0.2 to 0.001. The color scale is indicated by the color of the dots in Panel (b). In Panel (b), the main figure shows the RL magnetization at critical point $\mu(r = 0, h)$ as a function of h. The inset shows the corresponding susceptibility $\chi(r, h)$ near the critical point estimated through finite-difference scheme. No estimates are provided for $h = 0.2$. The dashed lines indicate the mean-field predictions Eq. (19).

the RL transition between the warm and hydrodynamics phases. In particular, it predicts the following magnetization profiles

$$\begin{aligned} &\mu(r, h = 0^+) = \sqrt{1 - r} \quad \text{if } r > 0 \ \text{ and 0 otherwise,} \\ &\mu(r = 0, h) = (3h)^{1/3}, \\ &\chi(r, h) := \frac{\partial \mu}{\partial h} = \frac{3}{r} \ \text{ if } r > 0 \text{ and } \frac{3}{2r} \text{ otherwise.} \end{aligned} \tag{19}$$

Fig. 8 shows that the lowest order predictions for the magnetization are in excellent agreement with the RL data. The spontaneous magnetization $\mu(r, h)$ indeed seems to converge towards the mean-field prediction as h is decreased towards 0. At the critical point, the scaling with h is close to perfect over two decades. This suggests that as $h \to 0$, the susceptibility $\chi(r = 0, h)$ indeed genuinely diverges, and that the RL transition is a continuous phase transition. However, we notice deviations from our mean-field prediction for the susceptibility. The mean-field exponent is compatible with the data, but a finer assessment would require reaching higher resolutions. We remark that the behavior of $\chi(r, h)$ in the hydrodynamic phase is seemingly independent of h, as predicted by Eq. (19). This is not the case in the warm phase and results in deviations from our heuristic mean-field predictions.

Our partial conclusion at this point is that in spite of the warm second-order deviations from the mean-field, Fig. 8 suggests that the RL transition between warm and hydrodynamic states indeed fits into a general thermodynamic framework and corresponds to a continuous phase transition. It is unclear whether specific properties of the transition could be deduced from first principles, but these considerations are beyond the scope of the present work.

D. From Reversible-Leith to Reversible Navier-Sokes dynamics

Even though the RL model has a very simple dynamics, it is naturally tempting to infer that the RNS statistics fits into a similar general thermodynamic framework as the one identified in the Leith case. We shall not refrain from doing so in § V, in order to explore a thermodynamic formulation of Gallavotti's conjecture that could have practical implications for its rigorous numerical assessment. Prior to this, let us however briefly point out some important differences between the RL and the RNS formulations.

a. $\mathcal{R}_\mathrm{L}$ vs. $\mathcal{R}_\mathrm{r}$.
The specific definition of the reversible control parameter is different in the RNS and RL formulations, being dependent on the reversible dynamics in the respective systems. Therefore, we do not expect the RL free energy Eq. (18) to account for the finite-size effects observed in our RNS numerics. We can investigate the RNS system in terms of the following redefined control parameter

$$\tilde{\mathcal{R}}_\mathrm{r} := \langle \epsilon_\mathrm{inj} \rangle^{2/3} \ell_f^{2/3} E_0^{-1}; \tag{20}$$

this would provide an exact analogue of the definition Eq. (13). This definition is more appropriate for a comparative study of the RNS system under different forcing schemes. The only drawback of such a definition is that it relies on a data-driven measurement, namely

that of $\langle \epsilon_{\rm inj} \rangle$. In the present work, we see this only as a minor issue, with no relevance for the forthcoming discussion. In our view, this is one of the reason why the RNS mean-field description fails to account for the RNS statistics in a strict sense. However, upon defining the RNS hydrodynamic magnetization as $\mu_{\rm RNS} := \tilde{\Omega}$ rather than the square-root RL definition Eq. (17), and using $r_{\rm RNS} := \mathcal{R}_{\rm r}/\mathcal{R}_{\rm r}^\star - 1$ as the RNS reduced temperature, it is apparent that the mean-field free-energy prescribed by Eq. (17) correctly accounts for the phenomenological square-root fit of Fig. 2. Note that higher-resolution runs are needed to examine the role of $k_{\max}$ on the RNS transition.

b. Dynamical behavior within the transition region. Another difference between the present RNS and RL formulations relates to the fact that the injected power fluctuates in time in the former. We think that this feature prevents the RL dynamics from having a noticeable transition region at finite $k_{\max}$. Specifically in the Leith model, for a given input flux ϵ_0 and prescribed finite $k_{\max}$ only one steady solution exists. It is either a warm solution or a hydrodynamic solution: In other words there is no multi-stability of solutions. This could well be the case in the RNS system, if the injected power was constant in time. However, in our RNS formulation the injected power $\epsilon_{\rm inj}$ is constant only on average. For the fixed total energy, the input parameter f_0 only imposes the upper bound: $|\epsilon_{\rm inj}| \leq 2E_0|f_0|$. The enstrophy fluctuations observed in the transition region for the RNS simulations could therefore be simply due to power fluctuations, selecting either a warm solution or a hydrodynamic solution as a function of the instantaneous value of $\epsilon_{\rm inj}$. These fluctuations therefore are not captured by the mean-field Landau description Eq. (17). Further intuitions on this matter could perhaps be obtained by generalizing the deterministic RL framework to a stochastic one, but this is beyond the scope of the present work.

It is insightful to use the RL analysis as a guiding framework, irrespective of the intrinsic differences between the RNS and RL systems, to interpret the RNS transition as a genuine continuous phase transition in the limit $k_{\max} \to \infty$. This has practical implications for the Gallavotti's *equivalence conjecture*, which we discuss in the next section.

V. TURBULENT LIMIT, CRITICAL POINT AND GALLAVOTTI'S CONJECTURE

So far, we have focused on the RNS statistics, without any reference to the standard NS statistics, except for some very qualitative comments. However, as explained in the introduction, the motivation in studying reversible dynamics is to assess whether Gallavotti's *equivalence conjecture* holds true. In essence, the conjecture states an identity between the RNS and NS invariant measures, hereafter denoted as $\langle \cdot \rangle_{E_0}$ and $\langle \cdot \rangle_\nu$, respectively. We quote directly from Ref. [33] and state the equivalence as an (asymptotic) statistical identity valid for a suitable class of observable $\mathcal{O}$, *e.g.*

$$\langle \mathcal{O} \rangle_\nu = \langle \mathcal{O} \rangle_{E_0} (1 + \circ(1)), \tag{21}$$

where $\circ(1)$ denotes a vanishing quantity in a suitable joint limit $\nu \to 0, k_{\max} \to \infty$ [54]. We will no further comment on the notion of a "suitable class of observables", except that the latter must contain the energy E, so that the following *reflexivity property* holds:

$$\langle E \rangle_\nu = E_0 (1 + \circ(1)). \tag{22}$$

The notion of a "suitable joint limit" $\nu \to 0,\ k_{\max} \to \infty$, however needs further substantiation. In Ref. [33], the authors consider the limit $\nu \to 0$ at fixed value of $k_{\max}$. This limit is particularly relevant in the perspective of the many interesting recent developments related to Galerkin-truncated dynamics [37, 38, 47, 55–57]. In this limit, it is now known that the NS equations generate quasi-equilibrium flows [58]. It is therefore not the relevant asymptotics in the context of describing fully developed turbulence, which the (truncated) NS equations in principle generate in the joint ordered limit

$$k_{\max} \to \infty \ \text{ first, } \ \nu \to 0 \ \text{ then,} \tag{23}$$

at fixed forcing statistics. Within the turbulent limit (23), the statistical identity (21) describes a dynamical equivalence between the *full* RNS and the *full* NS statistics. To the best our understanding, this also corresponds to the original formulation of the equivalence conjecture [25, 40].

Let us now explicitly assume that the RNS steady statistics are described by a continuous phase transition at $\mathcal{R}_{\rm r}^\star$ as $h := k_0/k_{\max} \to 0$. One can then precisely identify the turbulent limit as the critical point asymptotics, approached from the hydrodynamic phase.

A. Turbulent limit and critical point asymptotics: $\mathcal{R}_{\rm r} \to \mathcal{R}_{\rm r}^\star$ & $h \to 0$.

The identification of the turbulent limit as the critical point asymptotics is a consequence of the transition being continuous. Indeed, recalling the warm behavior $\langle \nu_{\rm r} \rangle \propto h^2 \to 0$ illustrated in Fig. 2 (a) and Fig. 7 (c), we infer that the reversible viscosity is uniformly vanishing for $\mathcal{R}_{\rm r} < \mathcal{R}_{\rm r}^\star$ in the limit $h \to 0$. Assumed continuity of the transition then yields $\langle \nu_{\rm r} \rangle = 0$ at $\mathcal{R}_{\rm r} = \mathcal{R}_{\rm r}^\star$. Besides, for example, assuming a constant energy E_0 as $\mathcal{R}_{\rm r} \to \mathcal{R}_{\rm r}^\star$, the forcing amplitude converges towards a finite limit, so that $f_0 \to f_0^\star := \mathcal{R}_{\rm r}^\star E_0/\ell_f$: We have recovered the turbulent limit (23).

We comment on two salient features of this thermodynamic reformulation of the RNS turbulent limit.

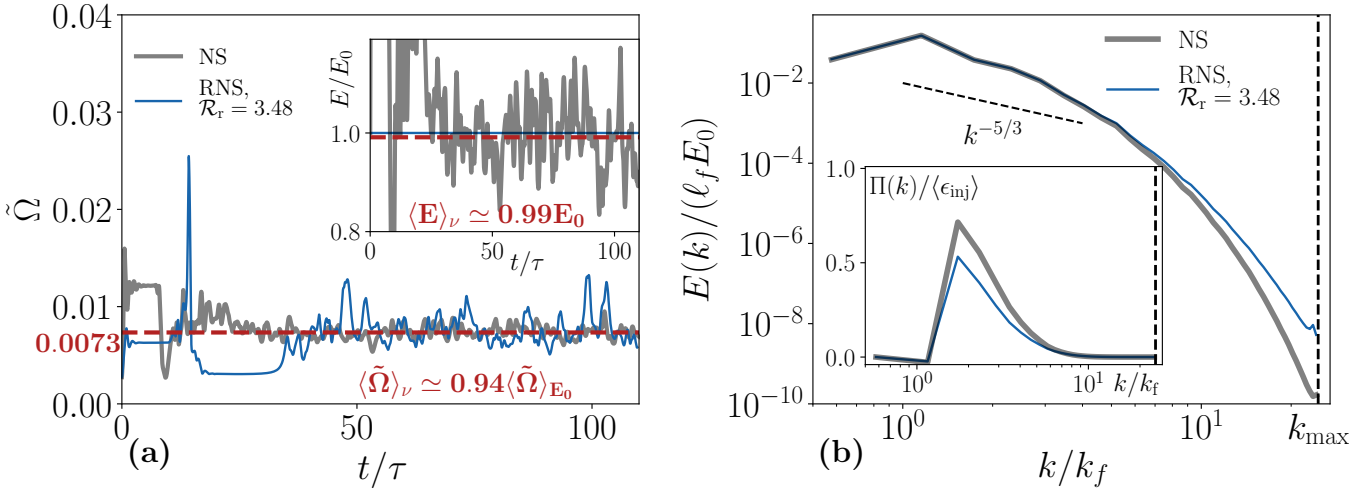

FIG. 9. **RNS *vs.* NS at $\mathcal{R}_r \gtrsim \mathcal{R}_r^\star$.** Panel (a) superimposes the times series of the normalized enstrophy (main panel) for the $\mathtt{B}_{128}$ RNS run at $\mathcal{R}_r = 3.48$ and a corresponding NS run, with same Taylor-Green forcing and standard viscosity set to $\nu = \langle \nu_r \rangle$. Inset shows the corresponding data for the energy time series, showing the validity of the reflexivity property (see text). The dashed-red lines indicate NS time-averages. Panel (b) compares the time-averaged energy spectra (main panel) and fluxes (inset) for both the RNS and NS runs. Kolmogorov scaling is indicated by a dashed line with label $k^{-5/3}$. E_0 is the conserved total energy of the RNS run.

a. Order of the limits:
In the limit $h \to 0$, the warm states are strictly speaking ill-defined as a consequence of the ultra-violet catastrophe, as partially explained in Appendix A. Hence, approaching the critical point from below necessarily requires taking the limit $\mathcal{R}_r \overset{<}{\to} \mathcal{R}_r^\star$ *before* $h \to 0$. In contrast, the hydrodynamic states are well defined even as $h \to 0$: We have extensively argued throughout our exposition that the statistics are independent of the cutoff in this phase. We therefore conjecture that approaching the critical point from above can therefore also be done by taking the thermodynamic limit *before* the critical limit; in other words, the limits $h \overset{>}{\to} 0$, and $\mathcal{R}_r \overset{>}{\to} \mathcal{R}_r^*$ should in principle commute. We can therefore unambiguously refer to the (unordered) joint limit $h \overset{>}{\to} 0$, $\mathcal{R}_r \overset{>}{\to} \mathcal{R}_r^*$ as the "turbulent limit".

b. Anomalous dissipation:
In the limit $h \overset{>}{\to} 0$, $\mathcal{R}_r \overset{>}{\to} \mathcal{R}_r^*$, we could in principle expect anomalous dissipation from the RNS statistics. This is yet better seen if the alternative definition $\tilde{\mathcal{R}}_r$ of Eq. (20) indeed could be used as a valid reversible control parameter. We will then obtain $\langle \epsilon_{\rm inj} \rangle \to \epsilon^\star := \ell_f E_0^{3/2} \tilde{\mathcal{R}}_r^{\star 3/2} < \infty$. This argument suggests that the scale-by-scale energy budget and the associated 4/5 laws could be deduced following the exact same steps as for the standard NS equations [13], hinting at the equivalence between those two dynamics at the critical point.

B. RNS *vs.* NS near criticality: Illustrative numerics

As a final illustration of the relevance of the joint limit $k_{\max} \to \infty$, $\mathcal{R}_r \overset{>}{\to} \mathcal{R}_r^\star$, let us here explicitly compare the RNS statistics from Set $\mathtt{B}_{128}$ to their NS counterpart at $\mathcal{R}_r \sim 3.48 > \mathcal{R}_r^+$, a value which corresponds to the lower end of the hydrodynamic regime for our resolution. As stated before, the RNS system then produces a non-trivial statistical state, which involves multitude of length and time scales. To generate corresponding NS steady states, we integrate the NS equations with same Taylor-Green forcing amplitude f_0 and set the standard viscosity to $\nu = \langle \nu_r \rangle$. The main results are summarized in Fig. 9. The inset of Panel (a) shows that the NS energy fluctuates around the imposed RNS value, *e.g.* $\langle E \rangle_\nu \simeq 0.99\, E_0$, and this reflects the approximate validity of the reflexivity condition prescribed by Eq. (22). The main panel shows that the NS and the RNS enstrophy time-series fluctuate around a similar mean value. The fluctuations are more or less commensurate with each other (slightly larger for the RNS run).

Fig. 9 (b) shows that the RNS and the NS dynamics in this regime have in fact similar large-scale features. In particular, both the spectra and the fluxes show excellent agreement on a decade of wave numbers ($k < 10k_f$), before starting to deviate in the ultra-violet range $k > 10k_f$. This is a consequence of our simulations having finite resolution, and these differences would probably disappear upon taking larger $k_{\max}$ for same f_0.

VI. CONCLUDING REMARKS

Time-reversible formulations of forced-dissipative hydrodynamical equations, addressing Gallavotti's equivalence conjecture of (hydro)dynamical ensembles have emerged in recent years as an important framework to provide an out-of-equilibrium thermodynamic perspective on the issue of turbulent irreversibility. Yet, in spite of many promising recent numerical results using reduced models, circumstances under which the equivalence conjecture might hold true remains unclear. Also, the attention has recently shifted to analyze (reversible) models wherein thermostats preserve various other quadratic quantities, and not necessarily the total energy. Within these frameworks, the equivalence conjecture has been assessed in the near equilibrium regime, which corresponds to the vanishing viscosity at finite resolution [33–35]. In the present work, we have followed a completely different route, in order to provide intuition on the potential validity of the equivalence conjecture for the full 3D dynamics, in the limit $k_{\max} \to \infty$, $\nu \to 0$. To this end, our analysis has focused on studying the dynamics of the RNS system that preserves the total kinetic energy. We carried out an extensive numerical study of the RNS system to fully explore its statistical regimes and also provide an illustrative comparison of the RNS and NS statistics. We find this approach particularly insightful.

Our numerics show that the RNS system undergoes a continuous phase transition controlled by a non-negative dimensionless parameter $\mathcal{R}_{\rm r} = f_0 \ell_{\rm f}/E_0$, which quantifies the balance between the fluctuations of kinetic energy at the forcing length-scale $\ell_{\rm f}$ and the total energy E_0; f_0 is the forcing amplitude. In our opinion, it is possible to use an alternative definition (data driven) of the control parameter, without modifying the overall picture: $\tilde{\mathcal{R}}_{\rm r} = \langle \epsilon_{\rm inj} \rangle^{2/3} {\ell_{\rm f}}^{2/3}/E_0$, where $\langle \epsilon_{\rm inj} \rangle$ is the stationary value of the injected power. For small $\mathcal{R}_{\rm r}$, the RNS dynamics produces a "warm" stationary statistics, *e.g.* characterized by the partial thermalization of the small length-scales and an intrinsic dependence on the cutoff $k_{\max}$. At large $\mathcal{R}_{\rm r}$, the stationary solutions have a hydrodynamic behaviour, characterized by compact energy support in k-space and are essentially insensitive to the truncation scale $k_{\max}$.

The transition between the two statistical regimes is observed to be smooth, with a narrow crossover range in the vicinity of $\mathcal{R}_{\rm r}^\star \simeq 2.75$. It is characterized by a highly bursty dynamical behavior of the enstrophy, whose fluctuations are commensurate with its mean. In this regime, the system exhibits multi-stability: It oscillates between a hydrodynamic-type low-enstrophy regime and a high-enstrophy regime, whose small length-scale statistics are yet far from being thermalized and exhibit non-trivial power law scalings. The enhancement of the enstrophy fluctuations in this transition region hints at a continuous phase transition between the warm regime and the hydrodynamic regime, with time-averaged reversible viscosity

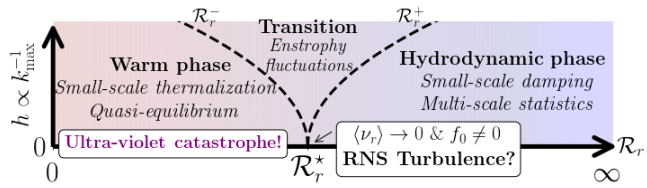

FIG. 10. A refined phase diagram for the RNS steady-state. Our numerical simulations suggest $\mathcal{R}_{\rm r}^\star \approx 2.75$.

(or equivalently normalized enstrophy) emerging as an order parameter. The transition in principle occurs only in the thermodynamic limit $k_{\max} \to \infty$. Therefore, a strict characterization of the transition must necessarily involve finite-size scaling analysis.

To further substantiate this idea, we used a simple one-dimensional non-linear "Leith-type" diffusion model, modified to preserve energy, so that it mimics the RNS system. The main difference between the RL and the RNS system is the forcing scheme, which in the former is imposed by requiring constant energy fluxes at the boundaries. RL formulation allows the computation of steady states without relying on the direct numerical integrations of the RL equations, but rather using a non-trivial parametrization and ideas from the theory of dynamical systems. Similar to the RNS analysis, the RL steady regimes were classified depending on a dimensionless control parameter $\mathcal{R}_{\rm L}$ and these mimic the smooth transition between the warm and hydrodynamics states.

The simplicity of the RL formulation allowed us to investigate in detail the finite-size effects and the related influence of the cutoff $k_{\max}$. This asymptotic analysis substantiated the idea of a continuous phase transition: In fact, we find that the signatures of the phase transition close to the critical point $\mathcal{R}_{\rm r}^\star$ can be obtained by constructing a heuristic mean-field Landau free energy. In this picture, $\mathcal{R}_{\rm r}$ indeed behaves as a thermodynamic control parameter, *e.g.* a temperature; the relevant order-parameter is defined in terms of a suitably normalized enstrophy, while the symmetry breaking parameter h is identified as the cutoff length-scale $1/k_{\max}$.

Naturally, the RL dynamics only reproduces the idealized features of the RNS transition and differs from the RNS system in important ways. In the Leith model, the critical control parameter is exclusively identified from the properties of the average steady state, and therefore it does not account for the dynamical signatures of the transition that are found in the RNS system, namely the enhancement of enstrophy variance in the vicinity of the critical point. Also, the high-enstrophy region ($\mathcal{R}_{\rm L} < \mathcal{R}_{\rm L}^\star$) exhibits close to thermalization spectra $E(k) \sim k^2$ up until $\mathcal{R}_{\rm L}^\star$; this is in contrast with the RNS observations, wherein close to the critical value

$\mathcal{R}_{\rm r}^\star$, the power-law exponents of the energy spectra at small length-scales are observed to fluctuate, but are bounded by 2. This signals a clear departure from the Gibbsian equipartition in the RNS system, and this is not captured by the simplified model. In our view, these differences can for the most part be traced back to the fact that the injected energy fluctuates in the RNS system, but is held constant in the RL model.

In spite of the above differences, it is quite evident that the RNS systems exhibits a continuous phase transition; therefore, the phase diagram is qualitatively similar to the one obtained for the RL model (Fig. 10). This makes it possible to examine the Gallavotti's equivalence conjecture by formulating the turbulent limit in terms of the critical point asymptotics $\mathcal{R}_{\rm r} \overset{>}{\to} \mathcal{R}_{\rm r}^\star, h \overset{>}{\to} 0$, with the overset symbol "$>$", where limit is approached from the hydrodynamic regime. We have argued that in this limit the RNS states should have anomalous energy dissipation and formally vanishing thermostat effects, thereby hinting at the validity of the conjecture; a comparison of the RNS and NS numerics indeed suggests that this is true. Moreover, we strongly believe that the limits $\mathcal{R}_{\rm r} \overset{>}{\to} \mathcal{R}_{\rm r}^\star$ and $h \overset{>}{\to} 0$ commute, compared to the standard formulation of the turbulent limit as $k_{\max} \to \infty, \nu \to 0$ in the NS equations, this will then constitute a major simplification, and hopefully will pave the way for systematic assessment of the equivalence conjecture in future studies.

In the present work, we have restricted ourselves to DNSs involving rather modest numbers of grid points (up to $N_c^3 = 128^3$) and our description is based on one point statistical quantities. The complete characterization of the statistical regimes of the RNS system with larger grid sizes is computationally very demanding, given that many of the runs require long temporal evolution. Yet, our results suggest to study the asymptotic behavior of RNS only at the transition, namely by letting $N_c \to \infty$ at fixed $\mathcal{R}_{\rm r} \gtrsim \mathcal{R}_{\rm r}^\star$. While we have provided the evidence that in this regime the RNS system correctly reproduces the macroscopic properties of the NS equations, a systematic asymptotic analysis is still desirable, to investigate the nature of the agreement at higher Reynolds number. Moreover, a careful investigation of more refined statistical properties, beyond the relatively low-order statistics considered here, is needed to complete the picture, but we leave it for future investigations.

Acknowledgments. Part of this work was granted access to the following computing grants: GENCI (Grand Equipement National de Calcul Intensif) grant numbers: A0042A10441 (IDRIS and CINES), A0062A10441 (IDRIS, CINES and TGCC) and 2A310096 (IDRIS). B. Dubrulle acknowledges funding from ANR EXPLOIT, grant agreement no. ANR-16-CE06-0006-01. S. Nazarenko is supported by Chaire D'Excellence IDEX, Université de la Côte d'Azur, France.

[1] C. Cercignani, in *The Boltzmann equation and its applications* (Springer, 1988) pp. 40–103.
[2] C. Cercignani, R. Illner, and M. Pulvirenti, *The mathematical theory of dilute gases*, Vol. 106 (Springer Science & Business Media, 2013).
[3] S. Chibbaro, L. Rondoni, and A. Vulpiani, Springer, Berlin **3**, 17 (2014).
[4] R. Zwanzig, Journal of Statistical Physics **9**, 215 (1973).
[5] R. Zwanzig, *Nonequilibrium statistical mechanics* (Oxford University Press, 2001).
[6] B. Turkington, Journal of Statistical Physics **152**, 569 (2013).
[7] C. Gardiner, *Stochastic methods*, Vol. 4 (springer Berlin, 2009).
[8] L. Onsager and S. Machlup, Physical Review **91**, 1505 (1953).
[9] L. Bertini, A. De Sole, D. Gabrielli, G. Jona-Lasinio, and C. Landim, Journal of Statistical Physics **107**, 635 (2002).
[10] H. C. Öttinger, *Beyond equilibrium thermodynamics* (John Wiley & Sons, 2005).
[11] J. Kurchan, Journal of Statistical Mechanics: Theory and Experiment **2007**, P07005 (2007).
[12] R. C. Kraaij, A. Lazarescu, C. Maes, and M. Peletier, Stochastic Processes and their Applications (2019).
[13] U. Frisch, *Turbulence: the legacy of AN Kolmogorov* (Cambridge university press, 1995).
[14] J. Berg, B. Lüthi, J. Mann, and S. Ott, Phys. Rev. E **74**, 016304 (2006).
[15] D. Buaria, B. Sawford, and P. Yeung, Phys. Fluids **27**, 105101 (2015).
[16] D. Buaria, P. Yeung, and B. Sawford, Journal of Fluid Mechanics **799**, 352 (2016).
[17] S. S. Ray, Physical Review Fluids **3**, 072601 (2018).
[18] H. Xu, A. Pumir, G. Falkovich, E. Bodenschatz, M. Shats, H. Xia, N. Francois, and G. Boffetta, Proc. Nat. Acad. Sci. **111**, 7558 (2014).
[19] H. Xu, A. Pumir, and E. Bodenschatz, Science China Physics, Mechanics & Astronomy **59**, 614702 (2016).
[20] A. Bhatnagar, A. Gupta, D. Mitra, and R. Pandit, Phys. Rev. E **97**, 033102 (2018).
[21] A. Pumir, H. Xu, E. Bodenschatz, and R. Grauer, Phys. Rev. Lett. **116**, 124502 (2016).
[22] J. Jucha, H. Xu, A. Pumir, and E. Bodenschatz, Phys. Rev. Lett. **113**, 054501 (2014).
[23] K. P. Iyer, J. Schumacher, K. R. Sreenivasan, and P. Yeung, arXiv preprint arXiv:1807.01651 (2018).
[24] Z.-S. She and E. Jackson, Phys. Rev. Lett. **70**, 1255 (1993).
[25] G. Gallavotti, Phys. Lett. A **223**, 91 (1996).
[26] G. Gallavotti and E. G. D. Cohen, Phys. Rev. Lett. **74**, 2694 (1995).
[27] G. Gallavotti and E. G. D. Cohen, J. Stat. Phys. **80**, 931 (1995).

[28] L. Biferale, D. Pierotti, and A. Vulpiani, J. Phys. A: Math. Gen. **31**, 21 (1998).
[29] L. Rondoni and E. Segre, Nonlinearity **12**, 1471 (1999).
[30] S. Aumaître, S. Fauve, S. McNamara, and P. Poggi, The European Physical Journal B-Condensed Matter and Complex Systems **19**, 449 (2001).
[31] G. Gallavotti, L. Rondoni, and E. Segre, Physica D: Nonlin. Phen. **187**, 338 (2004).
[32] S. Ciliberto and C. Laroche, J. Physique IV **8**, Pr6 (1998).
[33] L. Biferale, M. Cencini, M. De Pietro, G. Gallavotti, and V. Lucarini, arXiv preprint arXiv:1804.06273 (2018).
[34] G. Gallavotti, Private communication (April 2019).
[35] M. De Pietro, L. Biferale, G. Boffetta, and M. Cencini, Eur. Phys. J. E **41**, 48 (2018).
[36] C. Connaughton and S. Nazarenko, Physical Rev. Lett. **92**, 044501 (2004).
[37] C. Cichowlas, P. Bonaïti, F. Debbasch, and M. Brachet, Physical review letters **95**, 264502 (2005).
[38] G. Krstulovic and M.-É. Brachet, Physica D: Nonlinear Phenomena **237**, 2015 (2008).
[39] S. Thalabard and B. Turkington, Journal of Physics A: Mathematical and Theoretical **49**, 165502 (2016).
[40] G. Gallavotti, Physica D: Nonlinear Phenomena **105**, 163 (1997).
[41] P. Debue, V. Shukla, D. Kuzzay, D. Faranda, E.-W. Saw, F. Daviaud, and B. Dubrulle, Phys. Rev. E **97**, 053101 (2018).
[42] R. Kubo, Journal of the Physical Society of Japan **12**, 570 (1957).
[43] S. Thalabard and B. Turkington, Journal of Physics A: Mathematical and Theoretical **50**, 175502 (2017).
[44] G. Falkovich, in *Non-equilibrium statistical mechanics and turbulence*, edited by S. Nazarenko and O. V. Zaboronski (Cambridge University Press, 2008) Chap. 1.
[45] P. Yeung, X. Zhai, and K. R. Sreenivasan, Proceedings of the National Academy of Sciences **112**, 12633 (2015).
[46] E.-W. Saw, D. Kuzzay, D. Faranda, A. Guittonneau, F. Daviaud, C. Wiertel-Gasquet, V. Padilla, and B. Dubrulle, Nature communications **7**, 12466 (2016).
[47] G. Krstulovic, P. D. Mininni, M. E. Brachet, and A. Pouquet, Phys. Rev. E **79**, 056304 (2009).
[48] C. Leith, The Physics of Fluids **10**, 1409 (1967).
[49] C. Connaughton and R. McAdams, EPL (Europhysics Letters) **95**, 24005 (2011).
[50] S. Thalabard, S. Nazarenko, S. Galtier, and S. Medvedev, Journal of Physics A: Mathematical and Theoretical **48**, 285501 (2015).
[51] V. N. Grebenev, A. Griffin, S. B. Medvedev, and S. V. Nazarenko, J. Phys. A: Math. Theo. **49**, 365501 (2016).
[52] Similar feature is also observed in simulations of the truncated NS equations in the vanishing viscosity limit [58]. This result came to our knowledge during the revision of the present work.
[53] N. Goldenfeld, *Lectures on phase transitions and the renormalization group* (CRC Press, 2018).
[54] Asymptotic statistical identities such as (21) are exactly the kind involved in modern treatments of the equivalence between the canonical and the micro-canonical statistical ensembles, known to be valid for a wide class of systems in equilibrium statistical mechanics (see, *e.g.*, [59] and references therein).
[55] R. H. Kraichnan, Advances in Mathematics **16**, 305 (1975).
[56] U. Frisch, S. Kurien, R. Pandit, W. Pauls, S. S. Ray, A. Wirth, and J.-Z. Zhu, Phys. Rev. Lett. **101**, 144501 (2008).
[57] S. S. Ray, Pramana **84**, 395 (2015).
[58] A. Alexakis and M.-E. Brachet, arXiv preprint arXiv:1906.02721 (2019).
[59] H. Touchette, Journal of Statistical Physics **159**, 987 (2015).
[60] T. Lee, Quarterly of Applied Mathematics **10**, 69 (1952).
[61] R. H. Kraichnan, The Physics of Fluids **10**, 1417 (1967).
[62] R. H. Kraichnan, Journal of Fluid Mechanics **59**, 745 (1973).

Appendix A: Absolute equilibria of the truncated Euler equations

For $\mathcal{R}_\mathrm{r} = 0$, the numerical integration of the RNS equations exactly reduces to integrating the so-called "truncated Euler" equations. These are in fact obtained by performing a Galerkin truncation of the Euler equation at a cutoff wave number k_max. In practice, Galerkin truncations consist in suppressing all the triadic interactions involving wave numbers larger than k_max, whereby yielding a high-dimensional conservative set of non-linear ordinary differential equations. Truncated Euler flows exactly preserve the quadratic invariants of the original equations and satisfy a Liouville theorem. Hence, they typically converge towards thermal statistical states with Gibbsian statistics known as "absolute equilibria" [60–62], and the thermalization process usually exhibits interesting transients [37, 38, 47]. For the non-helical 3D truncated Euler flows that we consider in the present paper, the relevant absolute equilibrium state is particularly simple and prescribed by each Fourier velocity mode having independent centered Gaussian statistics with variance $\propto E_0/N_c^3$. This equilibrium state describes an equipartition of the total kinetic energy E_0 among the different modes. Assuming a continuous distribution of wave numbers, the corresponding energy spectrum can be estimated as

$$E_\mathrm{eq}(k) = \frac{3E_0}{k_\mathrm{max}^3} k^2, \tag{A1}$$

and the absolute equilibrium enstrophy is then

$$\Omega_\mathrm{eq} := \int_1^{k_\mathrm{max}} k^2 E_\mathrm{eq}(k)\,\mathrm{d}k \underset{k_\mathrm{max}\to\infty}{\sim} \frac{3}{5} E_0 k_\mathrm{max}^2. \tag{A2}$$

In the limit $k_\mathrm{max} \to \infty$, the absolute energy equilibria become ill-defined, as the resulting energy spectra cannot be normalized, unless they are trivial and the total energy is vanishing. This phenomenon is the so-called "ultraviolet catastrophe", which also prevents the warm RNS states to be properly defined in the limit $k_\mathrm{max} \to \infty$.